Imaging of protein distribution in tissues using mass spectrometry: an interdisciplinary challenge

*Jiaying Han[1,2], Hjalmar Permentier[1], Rainer Bischoff[1], Geny Groothuis[2], Angela Casini[2,3], Péter Horvatovich[1]**

[1]Analytical Biochemistry, Groningen Research Institute of Pharmacy, University of Groningen, Antonius Deusinglaan 1, 9713 AV Groningen, The Netherlands

[2]Pharmacokinetics, Toxicology and Targeting, Groningen Research Institute of Pharmacy, University of Groningen, Antonius Deusinglaan 1, 9713 AV Groningen, The Netherlands

[3]School of Chemistry, Cardiff University, Main Building, Park Place, CF10 3AT Cardiff, United Kingdom

Abbreviations

AP	atmospheric pressure
CID	collision-induced dissociation
CT	Computed Tomography
DCE	Datacube Explorer
DESI	desorption electrospray ionization
ECD	electron capture dissociation
ETD	electron transfer dissociation
ESI	electrospray
FAIMS	high field asymmetric waveform ion mobility
FFPE	formaldehyde-fixed and paraffin-embedded
FTICR	Fourier transform ion cyclotron resonance
H&E	hematoxylin and eosin
HCD	higher-energy collision induced dissociation
IHC	immunohistochemistry
IMS	ion mobility separation

IRMPD	infrared multiphoton dissociation
ISD	in-source decay
LAESI	laser ablation electrospray ionization
LA-ICP MSI	laser ablation inductively coupled plasma mass spectrometry imaging
LC/ESI-MS/MS	liquid chromatography electrospray ionization tandem mass spectrometry
LC-MS	liquid chromatography mass spectrometry
LID	laser-induced dissociation
MALDI	matrix assisted laser desorption ionization
ME-SIMS	matrix enhanced secondary ion mass spectrometry
MITICS	MALDI imaging team imaging computing system
MS/MS	tandem mass spectrometry
MSI	mass spectrometry imaging
NHS	N-hydroxysuccinimide
PC	photocleavable
3-SBA	3-sulfobenzoic acid
scFv	single chain variable fragment
SIMS	secondary ion mass spectrometry
SMALDI	scanning microprobe matrix assisted laser desorption ionization
4-SPITC	4-sulphophenyl isothiocyanate
TAMSIM	targeted multiplex mass spectrometry imaging
TMPP	N-succinimidyloxycarbonylmethyl)-tris(2,4,6-trimethoxyphenyl)phosphonium bromide
TOF	time-of-flight
UVPD	ultraviolet photodissociation

Abstract

The recent development of mass spectrometry imaging (MSI) technology allowed to obtain highly detailed images of the spatial distribution of proteins in tissue at high spatial resolution reaching cell dimensions, high target specificity and a large dynamic concentration range. This review focusses on the development of two main MSI principles, targeted and untargeted detection of protein distribution in tissue samples, with special emphasis on the improvements in analyzed mass range and spatial resolution over the last 10 years. Untargeted MSI of *in situ* digested proteins with matrix-assisted laser desorption ionization is the most widely used approach, but targeted protein MSI technologies using laser ablation inductively coupled plasma (LA-ICP) and photocleavable mass tag chemical labeling strategies are gaining momentum. Moreover, this review also provides an overview of the effect of sample preparation on image quality and the bioinformatic challenge to identify proteins and quantify their distribution in complex MSI data.

Introduction

Proteins participate actively in biological events and fulfill a wide range of molecular functions, such as substrate transport, cellular signaling, catalysis of metabolic reactions, and regulation of DNA replication and transcription events. Protein expression changes may indicate the presence and severity of a disease, and can be used to identify disease onset at an early stage, providing better treatment options for patients. Tissues are particularly important samples in clinical research, because they contain rich information on morphologic, metabolomic and proteomic changes related to biological events and disease pathology[1,2]. The imaging of protein distribution in tissues can provide new insights into the molecular mechanisms of diseases and the normal function of cells and tissues, as well as of aging processes. The spatial distribution of proteins in tissue samples provides information that is complementary to the relative and absolute concentration information obtained with commonly applied high-throughput molecular profiling omics approaches, such as liquid chromatography mass spectrometry (LC-MS)-based proteomics and metabolomics.

In order to obtain an image from a complex tissue specimen, several non-invasive imaging approaches have been developed such as radiography (X-ray, Computed Tomography (CT))[3], ultrasonography (USG)[4], positron emission tomography (PET)[5] and magnetic resonance imaging (MRI)[6] making use of different measurable physicochemical properties such as emitted/reflected light, particles (e.g. positrons) and ultrasound. These approaches have contributed significantly to the visualization of biological processes and many of them are applied routinely in clinical diagnostics. While many commonly used "non-invasive" (not requiring tissue sampling from patient) imaging technologies, such as CT and X-ray radiography, and "invasive" (requiring tissue sampling from patients) imaging technologies, including those based on ultraviolet-visible (UV-VIS) and fluorescence spectroscopy, are applied to provide high-quality images from tissues, this information cannot always be straightforwardly translated into an image reflecting the spatial distribution of individual analytes (e.g. proteins). Immunostaining in combination with optical or fluorescence imaging can provide signals from specific proteins by visualizing the distribution of antibody-antigen pairs in tissue. However, images acquired with UV-VIS, fluorescence and radiography[7,8] usually provide spatial distribution for only a limited number of proteins in a single experiment. In addition, most methods require *a priori* knowledge of the target molecules, which prevents their use as a hypothesis-free discovery and hypothesis-generating tool. Some imaging technologies measure the physicochemical properties of an ensemble of compounds, with spatial localisation in tissue such as nuclear magnetic resonance spectroscopy, or common UV-VIS microscopy[9,10], therefore, only inferring the presence of some compounds or classes of compounds. In this context, mass spectrometry imaging (MSI) is a powerful alternative, which circumvents some of these limitations.

In fact, MSI takes full advantage of the high chemical specificity of mass spectrometry and allow to quantify the spatial distribution of hundreds of individual molecules in tissues in a single measurement, without the need for labels or prior knowledge of the analytes. In addition, MSI technology allows to detect in one experiment multiple compounds which do not ionize well or are in low abundance, using reagents specifically targeting these compounds. Nowadays, there are several MSI approaches, which differ in the way that compounds are desorbed into the gas phase and ionized for sampling into the mass spectrometer, including secondary ion mass spectrometry (SIMS), MALDI MSI, LA-ICP MSI, desorption electrospray ionization (DESI), rapid evaporative ionization mass spectrometry (REIMS)[11], direct analysis in real time (DART)[12] and easy ambient sonic-spray ionization (EASI)[13]. Thus, the unique features of MSI to sample compounds directly allows analysis of many types of (bio)molecules such as proteins, metabolites and drugs, and provides potential for a wide range of research applications. Examples of these applications include approaches which provide new insight into normal and disease-related molecular processes[14,15,16], enable disease prognosis and prediction of response to therapy, allow to obtain the distribution of a drug in its intact form and its metabolites in tissue[17–20], or provide classification of tissues based on molecular information and reveal details of microbiome molecular communication[21].

This review focuses on state-of-the-art MSI approaches used to determine protein distribution in tissues. In details, the manuscript discusses the technical aspects of protein MSI, such as sample preparation, protein desorption in the gas-phase and ionization, spatial resolution and measured dynamic concentration range, and presents in detail various MSI approaches for targeted and untargeted detection of protein distributions in tissue samples. This includes the most commonly used untargeted protein imaging MSI using MALDI, and other ion generation and sampling approaches such as LA-ICP MSI, and targeted protein MSI using chemical labeling with photocleavable mass tags (e.g. Tag-Mass)[22–25]. One section discusses the data processing and interpretation challenge related to protein MSI. The review ends with a discussion of the possible future directions of MSI methodologies for protein distribution analysis in tissue samples.

1 Main steps of protein distribution analysis in tissue using mass spectrometry imaging

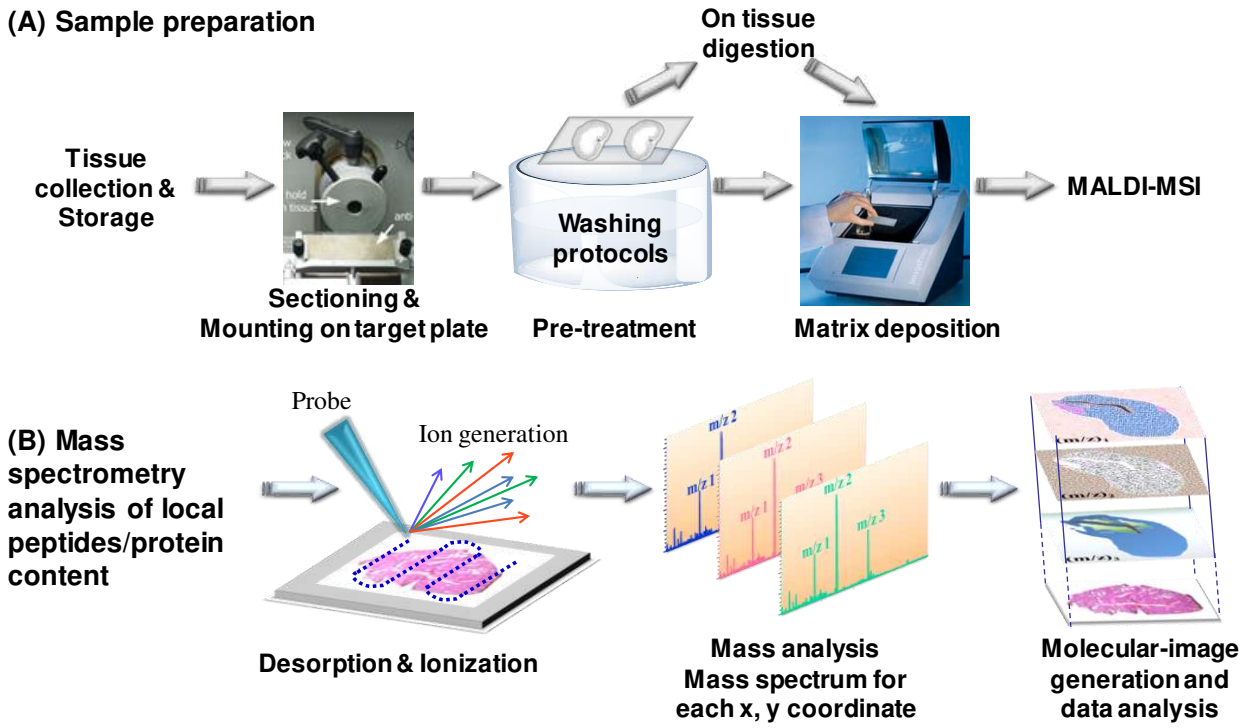

Figure 1. An example of mass spectrometry imaging (MSI) using a MALDI interface, which is a commonly used workflow for peptide/protein distribution analysis in tissue including tissue sectioning and sample preparation (A) and data acquisition and evaluation (B).

MSI of protein distribution in tissue samples consists of three main steps: sample preparation, data acquisition and data (pre-)processing and interpretation (**Figure 1**). The sample preparation protocols have a crucial impact on the quality of the MSI process. Sample preparation has the goal to facilitate the desorption into the gas-phase and the ionisation of proteins or peptides obtained after trypsin digestion, while keeping protein diffusion to a minimum and maintaining the original spatial distribution of proteins. These two aims are conflicting, and their balance plays a crucial role in the quality of the obtained MSI image. The mass spectrometer interface determines the desorption in the gas-phase, ionization and ion sampling efficiency, the speed of sampling and the area from which the ions are sampled. The latter property determines the theoretical spatial resolution of the MSI image. Theoretical spatial resolution can only be reached if sample preparation ensures that local protein abundance is maintained in the tissue to be imaged. The mass analyzer and acquisition parameters determine the speed of data acquisition, the type of registered spectra (with or without fragmentation), the measured dynamic range and the resolution of the acquired mass spectra. Bioinformatics solutions to pre-process and analyze MSI data form an important part of protein MSI workflows and have the

goal to interpret the large amount of collected protein distribution information together with other metadata such as a histology image with anatomical annotation by an expert pathologist[26,27].

1.1 Tissue sample preparation

Tissue sample preparation is probably the most critical step to obtain optimal sensitivity, reproducibility and spatial resolution of the protein distribution in an MSI experiments[28,29]. Inappropriate sample preparation leading to protein degradation, signal interference by non-target chemical species, alteration of the original protein distribution, or low ion sampling efficiency due to insulating properties of tissue have a negative effect on the quality of the acquired MSI data. Normally, tissue sample preparation involves organ harvesting and tissue sectioning (**Figure 1**). In order to avoid delocalization and degradation of proteins, it is essential to handle tissues correctly starting with the surgical removal process. After removal of the tissue from the body, tissue samples should be immediately snap-frozen in 2-methyl-butane (isopentane) and stored at -80 °C until use. For MSI of proteins, fresh frozen tissue is preferred over alcohol-preserved, or formaldehyde-fixated and paraffin-embedded (FFPE) tissue sections, because of the covalent crosslinking of proteins in FFPE sections or precipitated proteins in alcohol-preserved sections, although recently the antigen retrieval strategy has been suggested to overcome the protein crosslinks in FFPE sections[30,31]. In all cases, tissue sections with a thickness of approximately 10 µm are prepared with a microcryotome. It is important to place the frozen tissue sections on sample plates or conductive glass slides without scratches, rips or tears. Once the section (at this point still frozen) is in position, it is thaw-mounted by warming the bottom of the sample plate for macroscopic drying of the section which usually takes 20-30 seconds. Freeze-drying of tissue sections is an often performed operation, however many researchers omit this step from their tissue preparation pipelines without issue[32]. The sample plate and tissue section are quickly warmed together, resulting in no loss of water-soluble proteins nor translocation of the proteins due to diffusion in the liquid state[33].

Biological tissues contain numerous chemical species over a wide range of concentrations, and more abundant and/or easier ionizable species such as lipids can suppress the detection of less abundant species due to charge competition of compounds during ionization. For instance, salts and lipids[34] will interfere with MALDI MSI of proteins or peptides. To partially overcome these problems, tissue-washing procedures have been introduced prior to matrix deposition when using the MALDI MSI method. These washing protocols vary greatly depending on the target analytes. Ideally, all of the unwanted chemical species should be removed from the tissue while maintaining tissue morphology and not disturbing the original spatial distribution of soluble proteins. Assessment of all tissue-washing steps is necessary since each one may lead to some degree of disruption of the original spatial distribution of analytes in the tissue.

Matrix application is required for some of the approaches such as MALDI MSI or matrix enhanced secondary ion mass spectrometry (ME-SIMS) MSI. The most widely used technique for MSI is MALDI, for which the reproducibility of the ionization process is still a challenge and the MS acquisition parameters are difficult to optimize. Matrices such as 3,5-dimethoxy-4-hydroxycinnamic acid (sinapinic acid) and α-cyano-4-hydroxycinnamic acid are generally used to promote ionization and prevent degradation of target compounds by the probe beam (laser) energy. Generally, ion signal intensities in MALDI-MS are strongly influenced by the choice of matrix compound and the matrix preparation and deposition procedure, which determines the size distribution of the matrix crystals. Matrix crystal size is the most important parameter, which influences the ionization efficiency and reproducibility of desorption in the gas-phase of compounds. The goal of the procedure is to obtain a homogeneous distribution and uniformly small crystal sizes of matrix for optimal performance[35]. Several matrix application and drying cycles can be performed until an optimal matrix thickness with high quality and homogeneity is achieved. There are several methods by which a homogeneous matrix layer can be applied, such as spraying, solvent free dusting or coating by sublimation[36], and manual or robotic spotting[37,38]. Manual spraying is an often used, simple approach for matrix application which works well in the hands of an experienced operator, without requiring sophisticated instrumentation. However, automatic deposition provides a more homogenous matrix layer and improved reproducibility enhancing the imaging performance. The review by Goodwin on commonly used matrix and matrix applications approaches for MSI provides more details on this topic[29].

In MALDI MSI, proteins are measured with two approaches: either in their intact form, where smaller proteins are easier to measure than large proteins, or after digestion using a protease such as trypsin, which has the advantage that there is no limit with respect to protein size. Mass spectrometers with higher mass resolution allow to achieve better mass accuracy which improves identification of peptides and proteins. Moreover, since peptides are easier to detect and identify, this facilitates subsequent identification of proteins and their post-translational modifications. These two approaches are discussed in detail in sections 2.1.3 and 2.1.4.

1.2 Desorption and ionization of peptides and proteins from tissue

The choice of desorption (extraction into the gas-phase) and ionization technique has an important influence on the spatial resolution of the obtained MSI image and on the detected compound profile (**Figure 2**). SIMS is using high-energy primary ion beams of ionized noble gas, oxygen, fullerene or SF_6, to generate and to sputter secondary ions from sample surface. SIMS was introduced to MSI in the 1960s and was developed to detect atoms or small fragments of vitamins, pharmaceuticals, lipids and peptides in tissue and cells[39–41]. SIMS was applied to obtain information on elemental, isotopic and molecular composition of the upper atomic layers of the scanned sample[42,43]. It has the primary

advantage of achieving a high spatial resolution (< 100 nm or even ⩽ 20 nm), which cannot be achieved with MALDI, LDI or DESI interfaces[44,45,54–57,46–53]. However, SIMS suffers from severe in-source fragmentation of biomolecules due to excessively hard ionization, which results in impaired identification of target analytes. The lower sensitivity of SIMS-MSI in comparison to MALDI MSI in detecting peptides and proteins was reported in several studies[58].

DESI is an ambient ionization technique developed by Zoltán Takáts, Graham Cooks and their coworkers in 2004 at Purdue University[59,60]. In this method, a fast, nebulized electrospray gas jet transports charged microdroplets of an eluent to impact the surface of the sample and to carry away ionized molecules. The approach requires no or limited sample preparation effort and allows simple MSI under ambient conditions preventing change in tissue slice shape. Furthermore, DESI is a spray-based soft ionization technique with an average internal energy deposition of ~2 eV, which is similar to the internal energy deposition of electrospray (ESI)[61]. Thus, DESI yields minimal fragmentation of large molecules compared to the excessive fragmentation of SIMS[62] and avoids interference with the matrix compounds, such as observed in MALDI. DESI MSI and other variants, such as nano-DESI, have been used for imaging compounds in the low mass region below 1000 Da with a high spatial resolution (approximately 10 μm), as shown for metabolites in leaf tissues or drugs (e.g. clozapine) distribution in animal tissue sections and microbiome sampling[18,63–67]. The spot size and spatial resolution in (nano)-DESI-MSI – amongst other parameters – depend on the capillary diameter, angle of spray incidence and the tip-to-surface distance, which can be difficult to optimize[68]. (nano)-DESI MSI suffers from the limitation of a much lower spatial resolution compared to SIMS and MALDI, which is for (nano)-DESI typically around 100 μm or upwards in imaging of peptides or proteins[69–72]. Recently, Garza *et al.* presented a DESI-high field asymmetric waveform ion mobility (FAIMS) device for protein mass spectrometry imaging and reported to simultaneously detect lipids and intact protein forms in mouse kidney, mouse brain, and human ovarian and breast tissue samples[73].

Another ambient ionization method is laser ablation electrospray ionization (LAESI)[74,75], which was introduced by Vertes *et al.* in 2007 and combines laser ablation with a mid-infrared laser and electrospray ionization, where the latter serves to ionize the laser ablated compounds[74]. LAESI does not require complex sample preparation for MSI of peptides or proteins. However, it also suffers from low lateral resolution, which does not allow detailed (sub)cellular imaging.

It is necessary to find a technology to overcome all of the above-mentioned issues that can be used for imaging protein distributions in tissue samples. In this context, currently three MSI approaches are used: (1) untargeted MSI of proteins using MALDI, (2) targeted MSI of proteins based on detecting metals ions in their active sites or structural domains or metal ions coupled to antibodies using LA-ICP MSI such as used in mass cytometry, and (3) targeted MSI of proteins using chemical

labeling, where the chemical label consists of a protein targeting affinity moiety (antibody, affirmers, activity probes) coupled with photocleavable (PC) mass tags, where mass tag labels are released and measured with MALDI or LDI.

MALDI was the first MS-based method for imaging intact proteins in a human glioma[76] and is currently by far the most commonly used untargeted MSI approach for imaging protein distribution[77,78]. The first application of MALDI MSI in mapping peptides and proteins in biological samples was developed by the groups of Bernard Spengler (1994)[79] and Richard Caprioli (1997)[80]. MALDI MSI has since become a mature technology to determine the distribution of proteins over a large mass range from hundreds of Da to beyond 100 kDa with little or no fragmentation of the original protein[81,82,83–85]. During the last decade, MALDI imaging has been further improved, with respect to detection sensitivity and spatial resolution[86,87–91]. Current methods can reach a spatial resolution of 10-20 μm[84,92], a value that is limited by the crystal size distribution of the matrix, and therefore does not reach the typical spatial resolution of 100-250 nm of (nano)SIMS. In a typical MALDI MSI interface, ions are formed under vacuum, which constraints the choice of matrix, and may change tissue section morphology. To overcome these problems, atmospheric pressure MALDI (AP-MALDI) ion sources have been developed for MSI applications, where ions are generated at ambient conditions and transferred into the vacuum of the mass analyzer using methods similar to those developed for introduction of ions generated via ESI. AP-MALDI MSI using IR or UV lasers provides high spatial resolution (1.4 μm) in mapping small biomolecules, such as metabolites, lipids, peptides and carbohydrates, but has so far not been applied for protein MSI[93–97]. In addition, lower sensitivities are observed with AP-MALDI than with vacuum MALDI sources in analyzing plant metabolites[98].

Technique	Schematic	Mass range (Da)	Resolution (µm)	Benefits	Challenges
SIMS	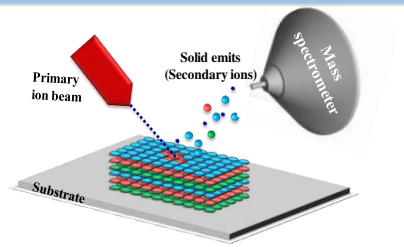	Dynamic SIMS 1-300 Static SIMS 100-1,500	Dynamic SIMS 0.03-0.5 Static SIMS 0.5-50	- high lateral spatial resolution - deep tissue profiling - low LOD* - low depleted material - quantitative imaging (dynamic SIMS)§	- source-induced fragmentation - small sampling area - need for conductive mounting surface (need for insulation) - stability of sample under UHV*
MALDI	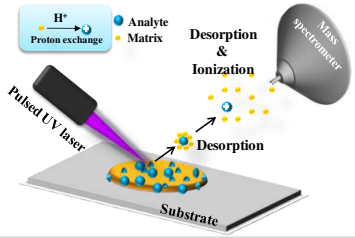	300-200,000	20-500	- wide mass range - AP* and IP* ion sources available - tolerance for large sampling area	- matrix interference - need for conductive mounting surface (needed for insulation) - inaccurate quantitative imaging - inability to measure low m/z (< 300)
DESI	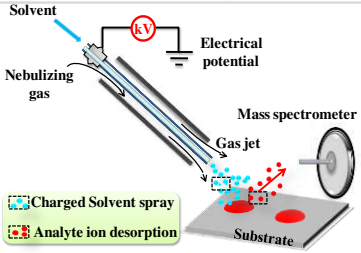	100-200,000	100-1,000 NanoDESI 10-1,000	- soft ionization - real-time imaging of dynamic processes - allow ionization under AP	- low lateral spatial resolution - inaccurate quantitative imaging - need for conductive mounting surface (need for insulation) - high gas pressure altering sample surface - information on elemental and atomic-cluster
LA-ICP	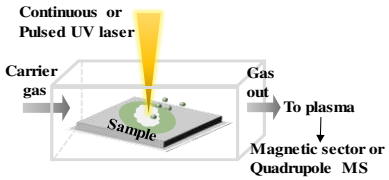	trace elements and specific isotope distribution of metal ions in proteins	10-100 µm	- low limit of detection (<µg g^{-1}) - wide dynamic quantification range	- elemental fractionation - interfering matrix effects
Mass tag	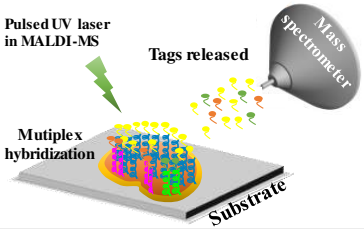	50-2000 - detection of large membrane proteins	10−100 µm	- no need for matrix - no mass range limitation	- requirement of expensive reagent - inaccurate quantification due to losses during chemical reaction and instability of the PC-linker during sample treatment

Figure 2. The main characteristics of desorption (extraction in the gas-phase) and ionization interfaces used for mass spectrometry imaging. Abbreviations: LOD: Limit of detection; AP: Atmosphere pressure; IP: Intermediate pressure. UHV: Ultra-high vacuum. *Static SIMS MSI detection of intact molecules above 1,500 Da from biological samples is rarely reported owing to source-induced fragmentation and high LOD for peptides and proteins. LAESI combining DESI and LA for desorption-ionisation was not included in the figure.

Other laser irradiation-based desorption/ionization MSI interfaces have been used in protein MSI besides those mentioned above, such as matrix-assisted laser desorption electrospray ionization (MALDESI)[99], and infrared laser desorption electrospray ionization (IR-LDESI)[100]. LA-ICP MSI is another popular approach used for imaging trace elements (e.g. metals and metalloids) in biological materials with a spatial resolution ranging from 200 μm down to 10 μm for a wide range of applications, among them visualization of metal-containing proteins[101–103].

1.3 Data processing and analysis

1.3.1 Spatial resolution in MSI

Spatial resolution is a key parameter to assess the performance of MSI. Spatial resolution is defined in the imaging field as the ability to distinguish two data points with different information content separated in units of distance such as mm or μm. Current MSI technology is able to provide data at low and submicron resolution, however, the spatial resolutions of 10-50 nm[104] achieved by super-resolution imaging is still not achievable. The term spatial resolution is used in multiple contexts, which often leads to confusion. The concept and definition of spatial resolution in the context of MSI is provided here. In general, a tissue is a three-dimensional (3D) compartment, whose MS imaging also provides 3D data, with three coordinate dimensions in tissue and one mass spectrum for each spatial coordinate. A general imaging approach such as MRI, PET or CT collects information on the entire 3D volume of data and in this context two types of resolution are defined: in the axial and the lateral dimension. Axial (longitudinal, azimuthal, range, radial, and depth[105]) resolution is defined in parallel to the probe beam of electrons, ions, or photons and defines the ability to distinguish structures at various depths of the sample with respect to the tissue surface[106].

Conversely, lateral resolution is defined perpendicular to the probe beam and defines the ability to distinguish structures which lie close to each other side by side, as individual objects. Lateral resolution is affected by the width of the beam, the difference between two adjacent coordinates (step size of sampling) at the tissue surface, but also depends on the depth of imaging i.e. the distance that the beam penetrates the tissue surface, since compounds are sampled from a tissue volume reached effectively by the sampling beam. Wider beams typically scatter in the tissue section and therefore, lateral resolution is improved by using narrower beams and beams that do not penetrate the tissue to great depths[107]. MSI is a surface scanning technology, with a low penetration depth into the sample, which is generally applied to a tissue section of a few μm thickness. Therefore, lateral spatial resolution in the plane of the tissue section is the important resolution parameter and this is the definition of spatial resolution used in this review. MSI techniques which acquire data from 3D

samples achieve this by merging mass spectrometry ion intensity data from adjacent tissue sections[108–112].

Spot size, pixel size and step size are important terms to describe the lateral resolution obtained in MSI. Spot size refers to the focus area of the probe beam (laser pulse, ion beam, etc.)[113], which has two definitions; one is based on a Gaussian distribution model of the beam intensity, or irradiance, across its standard deviation, while the second definition expresses the width of the beam at half-intensity[114,115]. Pixel size refers to the lateral binning (summing up intensity between a predefined set of borders) of 2D data into digital image elements and the step size refers to the raster of the sampling stage or beam deflections[57]. Step sizes smaller than the spot size were found to generate lower quality images when sampling with a laser which does not ablate all ionizable compounds from one spot. In this case, the tissue area is sampled with high overlap in adjacent sampling positions and sampling from the subsequent spot will result in some signal from compounds of the previous spot position. This is called oversampling. When the sampling area is completely ablated at each position without oversampling, the overlapping position will not be cross contaminated and leads to a clear image. In this case the resolution of the image is determined by the step size, since for each spot the sampled ions originate from the non-overlapping and non-ablated sample area. For this situation the lateral resolution is not limited by the diameter of the probe beam, but the intensity of the sample compound will be lower due to the lower amount of available material in the non-ablated sample area[116,117].

1.3.2 Pre-processing and visualization of large MSI data

The data pre-processing, visualisation and interpretation depends on the dimensionality of the MSI data. Tissue specimen has 3 dimensions (3D), from which a planar 2-dimensional (2D) tissue section with defined thickness (generally 5-10 μm) is used for MSI. Orientation of the tissue section used for MSI should be provided by sampling using an anatomical orientation description[118]. If multiple adjacent tissue sections are analyzed then volumetric MSI data is acquired[119]. The dimensionality of the MSI data is generally reflected as the spatial dimensions of the analysed tissue, thus it can be 2D or 3D. MSI data obtained from a single tissue section is multidimensional with two spatial, one separation (*m/z*) dimension and one quantitative readout (ion intensity). The two spatial dimensions are in the plane of the analysed tissue section and the separation dimension consist of the mass-to-charge (*m/z*) separation. The ion intensity is the quantitative readout, which is used for quantification of the measured compounds.

"Pseudo" MSI data can be obtained by taking individual samples at different parts on an organ, the full body or body surface and analyzing the samples with LC-MS or MALDI time-of-flight (TOF). Mapping the measured data to the original sample location enables coarse mapping of compound

distribution in the analyzed samples, as shown in a study measuring metabolites, peptides and proteins in samples taken from skins of volunteers by Bouslimani *et al*[120].

The size of the MSI data collected on large tissue sections at high spatial resolution is large and ranges typically from 1 to 100 GB and in extreme cases can reach 1 TB such as for 3D FTICR data, but smaller data sets of a few to hundreds of MB targeting small tissue areas with low spatial resolution is collected routinely. There are many ways to pre-process, analyze and evaluate the large amount of MSI data, and the main aims are to obtain a better understanding of the underlying molecular mechanisms of biological events such as: (1) to determine the spatial distribution of compounds and how this correlates with the anatomic morphology and cellular composition of the tissue, (2) to determine how the spatial distribution of a particular compound correlates with those of the other compounds. In the data interpretation process, visualization plays an important role, which is challenging for the large amount of MSI data, but large data sets represent a challenge for pre-processing as well. In order to reduce the volume of data, many data pre-processing pipelines use data reduction techniques such as centroiding, noise reduction, intensity filtering and baseline removal, creating images for features (isotopes) detected in a minimum number of spectra or filtering out ion images that have low information content[121,122].

Suits *et al.*[123,124] presented an approach which does not use any data reduction and allows to process large volume profile MSI dataset as it was collected. This is achieved by using three different types of indexed data structures of the same MSI data to allow interactive data interpretation by the users without loss of information (**Figure 3**): (1) one representation contains sliced MSI data in the *m/z* dimension with user defined thickness for fast visualization of MSI ion images, and enables correlation queries between slices to find compounds that show spatial correlation with each other or with an anatomical location, (2) representation of all MSI data in triplets of *m/z*, intensity and pixel index. In this data, triplets are sorted and indexed according to *m/z* values, which serves to recalculate a slice in the *m/z* dimension quickly with user defined thickness and *m/z* limits using a graphical user interface, and (3) indexed storage of all MS spectra of each image pixel serving to quickly get MS spectra for a particular tissue location.

The next level of data analysis is based on clustering similar mass spectra to determine how the spatial distribution of the mass spectra clusters correlates to anatomic structures, a process called segmentation. Another bioinformatics task is the alignment of the histology image with MSI data, which transfers identified anatomical regions in the histology image to the MSI data and enables identification of compounds in the identified anatomical region. This procedure is called the image registration process and performs 2D alignment of the histology image to e.g. a specific *m/z* slice or to the total ion current image (the sum of all ion intensities collected for one pixel) of MSI data[125].

Visualization of 2D MSI data obtained from one tissue slice is already challenging since one pixel is described with four values (x and y coordinates, *m/z* value and intensity) and the most common approach is to provide 2D images of single (normal image showing intensity as a color map) or multiple (separate red, blue and green color maps combined with intensity dependent transparency for 3 different slices) *m/z* slices. Visualization of ion intensity for a particular *m/z* range in 3D MSI data obtained from a volumetric sample or visualization of multiple *m/z* slices in 2D MSI can be performed with volumetric rendering frequently used in 3D computer graphics. Volumetric rendering is a 3D visualization method for 4D data where the color and the transparency of one pixel is set according to its intensity values (pixels with lower intensity are more transparent than pixels with higher intensity)[109].

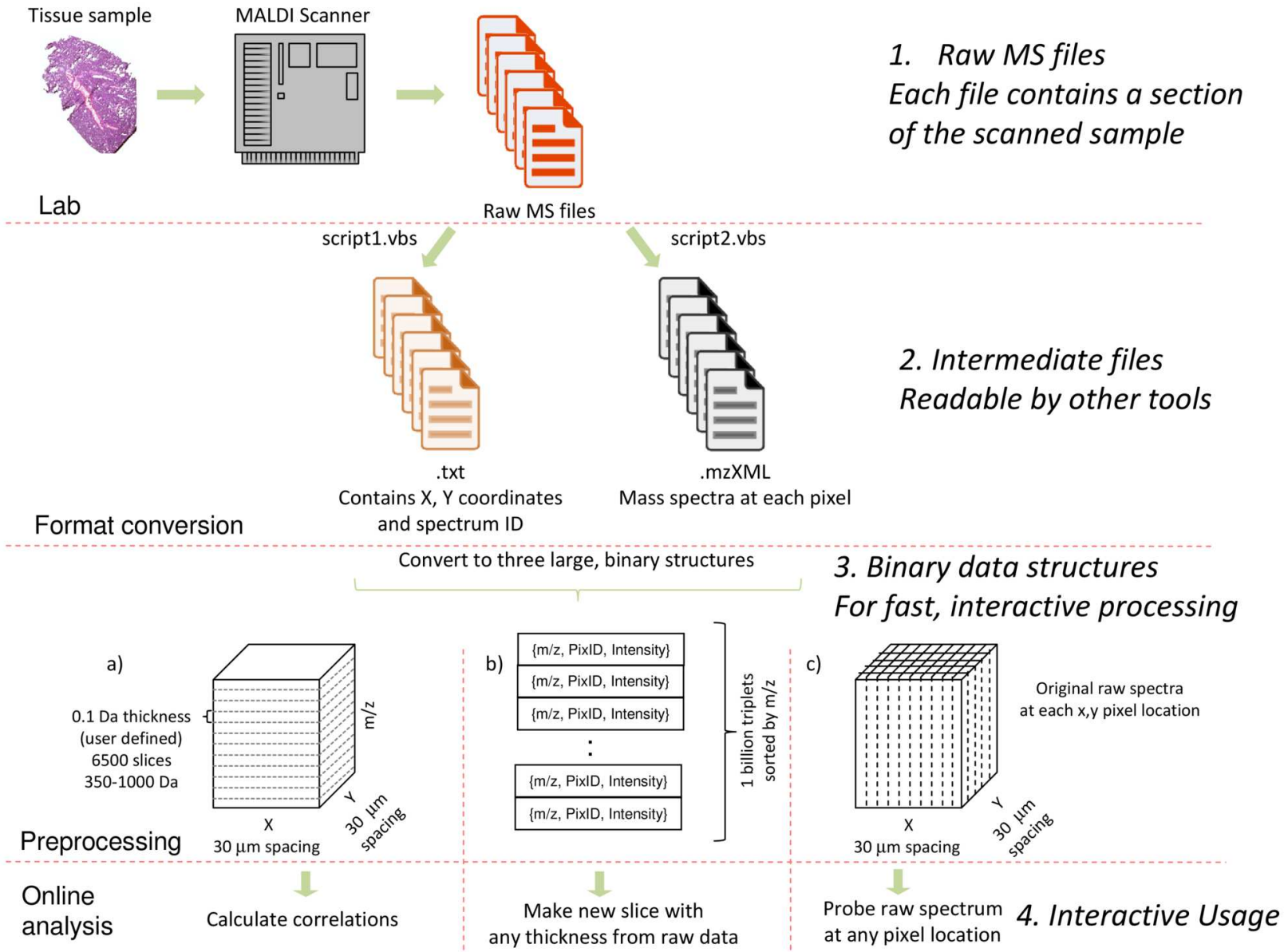

Figure 3. Data processing workflow, which allows analysing of all signals collected in an MSI experiment using an Orbitrap Velos instrument equipped with a MALDI interface interactively without information loss. Reprinted with permission from Suits *et al*[123]. Copyright (2013) American Chemical Society.

Identification of the detected peptides and proteins by MSI is still challenging, for instance due to the presence of isobaric compounds, poor fragmentation of large proteins, the presence of metabolites, adduct formation and the presence of non-tryptic peaks when local trypsin digestion is performed on the tissue section. Improvement of mass spectrometer sensitivity will allow detection of lower abundant proteins, but may actually exacerbate the identification challenge by increasing spectrum complexity. With a tandem mass analyzer, ions of interest can be specifically targeted for fragmentation, to facilitate their identification. However, tandem mass spectrometry (MS/MS) spectra of sufficient quality can only be obtained for ions with high intensity signals. An open non-reviewed database, the MSiMass list (https://ms-imaging.org/wp/msi-mass-list), helps users to assign identities to peaks submitted to MS/MS fragmentation observed in MALDI MSI experiments. This database is the result of a community effort without a formal review panel and therefore information in this database should be considered with care. In this concept, authors can freely enter data and can comment on existing entries. Its ability to provide high quality data and identification is currently under evaluation[126]. In this section we have mentioned only the most important aspects and challenges of MSI data processing and the reader is referred to a recent detailed review by Alexandrov on this topic[127].

MSI data is acquired with a wide range of MS systems and many software tools are available to process MSI data. For MSI data processing, imzML[128,129] is the accepted open standard format, which is supported by the Proteomics Standards Initiative of the Human Proteome Organisation (HUPO-PSI)[130], and has become widely used for the flexible exchange and processing of MSI data between different instruments and data analysis software. High-resolution molecular profiles of tissue collected from MSI experiments often have data files of sizes of several tens to hundreds of gigabytes requiring powerful visualization software, such as the Biomap (Novartis, Basel, Switzerland, www.maldi-msi.org) image processing application, the MALDI Imaging Team Imaging Computing System (MITICS)[131] and the Datacube Explorer (DCE, available at the www.imzml.org) to explore imaging mass spectrometry data sets[132]. Recently, high-quality 3D MALDI and DESI benchmark MSI datasets in imzML format were made available for software evaluation purposes[133].

2 Untargeted mass spectrometry imaging of proteins

This section discusses MSI strategies for hypothesis-free untargeted analysis of protein distribution in tissue and presents the technological limitations and current challenges, illustrated with example applications. Untargeted analysis of protein distribution requires the collection of ion intensity signals specific to proteins and linking accurate identification to these signals. In untargeted MSI, proteins can be identified with two approaches. In the first approach the proteins are digested *in situ* by

application of a protease (typically trypsin) in isolated spots, and the proteins in these spots are cleaved into peptides. These peptides are then ionized, sampled into the mass spectrometer and analyzed intact or following fragmentation using conventional MS/MS fragmentation methods such as collision induced (CID) or electron transfer dissociation (ETD). The application of droplets limits the spatial resolution of this approach. The second approach uses ionize, sample into the mass spectrometer and analyze intact proteoforms, which can be combined with fragmentation methods such as higher-energy collision induced dissociation (HCD) and ETD that can be directly applied to intact proteins extracted from tissue and submitted to purification[134–136]. The first strategy does not provide information on the entire protein sequence, and the detected peptides in many cases do not allow differentiation between protein isoforms or partially degraded proteins in the absence of additional information (e.g. the mass of the intact protein). Top-down fragmentation of intact protein provides more complete information on the entire protein sequence and allows better discrimination between isoforms, but requires clean and extracted proteins and cannot be applied directly in an MSI setting. The advantage of the first approach is that it can be applied to determine the distribution of post-translational modifications of specific residues in proteins directly from tissue[137].

2.1 Untargeted MALDI MSI of intact proteins in tissue

2.1.1 Extending the mass range for intact protein MALDI MSI

The matrix deposition method has a critical impact on the mass range of intact protein MSI. Leinweber *et al.* developed a sandwich matrix deposition protocol, which includes application of different solvents and detergents for MALDI MSI of proteins in tissue sections, extending the mass range to 25-50 kDa and increasing the number of detected intact proteins. This protocol uses two layers of matrix, one below and one on top of the tissue section, and has been employed for MSI of proteins in kidney, heart, lung and brain tissue sections of different rodent species[138]. Grey *et al.* introduced a tissue preparation procedure, which includes extensive washing with water to remove highly abundant water-soluble proteins, and automated spotting of matrix solution using a high percentage of organic (acetonitrile) solvent. This protocol allowed to measure membrane proteins up to 28 kDa in bovine lens, human lens, and rabbit retina by MALDI MSI, but at moderate spatial resolution of 100-200 µm due to application of matrix spotting[139]. Franck *et al.* enhanced the solubilization of large proteins using hexafluoroisopropanol (1,1,1,3,3,3-hexafluoro-2-propanol) and 2,2,2-trifluoroethanol during sample preparation and achieved MSI of proteins between 30 and 70 kDa directly from tissue[140]. Mainini *et al.* investigated ferulic acid as matrix on different tissues deposited with an automated matrix deposition device, ImagePrep (Bruker Daltonics, Bremen, Germany), which performs matrix deposition by spraying sequences and allowed the detection of proteins up to 135 kDa[141].

The shortcoming of widely-used mass spectrometers is the inefficient transmission and fragmentation of large proteins[138,140–144], particularly the low transmission efficiency of the latter. Recent development of mass spectrometers has enabled the implementation of large protein analysis even under native conditions by enhancing the ion transmission of intact proteins up to one megadalton[145]. These developments have allowed to expand the mass range within which intact proteins can be analyzed and will certainly contribute to generate more informative MSI data.

Another improvement of MSI of intact proteins was achieved by van Remoortere *et al.*, who used a high mass HM1 TOF detector (CovalX, Zurich, Switzerland) to improve the sensitivity of MALDI MSI of intact proteins up to 70 kDa[146]. Compared with traditional micro-channel plate detectors, this instrument has a much larger charge capacity and is therefore less prone to detector saturation. Another novel method in MALDI MSI was described by Jungmann *et al.*, who used a parallel, active pixel TOF detector for MSI of ubiquitin oligomers reaching a molecular mass of 78 kDa[147].

Although these methods demonstrate encouraging results for imaging proteins of increasing mass, each of these protocols has some drawbacks that are usually associated with low reproducibility, including: ion suppression effects[148], low ion yield (it has been estimated that only 1 molecule ionizes out of 1000 desorbed proteins[149–151]), the need for a special non-commercially available mass analyzer[146], a limitation to detect membrane proteins[139], the requirement of complex and laborious experimental protocols[138] and time-consuming, as well as extensive sample preparation[140].

2.1.2 Spatial resolution improvement of MALDI MSI for intact proteins

A number of methods were developed to implement the spatial resolution of MALDI MSI of proteins from tissue samples. These methods focused on improving the sample preparation protocol, reducing the laser beam spot size, and improving the ion sampling and transmission parts of the mass spectrometer. As mentioned in section 2.1.1, tissue sample preparation is the most important factor to achieve both high sensitivity and high spatial resolution in MALDI MSI. McDonnell *et al.* performed an extensive comparison of five tissue washing protocols using human arterial tissue samples, and assessed the methods in terms of the information content (e.g. number of detected peaks, quality of morphological structures) as well as their suitability for analyzing tissue containing small but distinct regions. In this work, they demonstrated an optimized tissue washing protocol using 70% and 90% isopropanol for imaging proteins that are specific to the *intimas* and *media* layers of atherosclerotic arterial tissues at a high spatial resolution of 30 μm[152]. With an appropriate laser spot profile (flat-top) and diameter (10-20 μm) and a matrix application method (spraying matrix with the Bruker ImagePrep device) that precludes analyte delocalization and maintains the original lateral spatial distribution of proteins, the group of Pineau reported a MALDI MSI of proteins in the 10 kDa range in rat testis tissue at 20 μm lateral resolution[136]. Caprioli's group implemented a matrix

sublimation/recrystallization process, which provides a more homogeneous distribution of the matrix resulting in more sensitive detection of large proteins using MALDI MSI with a spatial resolution as low as 10 µm[84]. Additionally, for targeted analysis, histology-directed imaging was performed using this protocol, where MSI analysis and hematoxylin and eosin (H&E) staining were performed on the same tissue section which was previously used for MSI. Integrating H&E staining with MSI data acquired on the same tissue section allows to transfer anatomical annotation from H&E staining to MSI data and allows to identify protein signals which correlate spatially with anatomical features. In another study, Deutskens *et al.* applied a robotic spray apparatus for matrix application, and performed MALDI MSI on a tissue section followed by elimination of the matrix by washing and subsequent histology staining and microscopic examination of the same tissue section. This matrix application protocol has two steps (one dry matrix coating and one hydration/recrystalisation), which separates the processes of matrix coating from analyte extraction and provides a highly reproducible homogenous matrix layer. A key advantage of this protocol is that it limits the delocalization of proteins and enables imaging at a relatively high spatial resolution of 35 µm[153].

The spatial resolution achievable with MALDI is ultimately restricted by the size of the laser spot[154]. While it is possible to image with a spatial resolution less than the diameter of the laser beam by oversampling (i.e. with a laser spot size of 60 µm, one could raster with 20 µm steps) to effectively achieve 20 µm spatial resolution[116], it is important to completely ablate the prior spot before moving the laser beam to the next position to reduce crosstalk between pixels. To minimize the laser spot size, the group of Caprioli *et al.* developed a new source for MSI with a transmission geometry that allows the laser beam to irradiate the backside of the sample and the separation of ion and laser optics resulting in a laser spot size close to the wavelength of the applied laser, thereby allowing MSI at higher spatial resolution. This method produced high-quality images of intact insulin in the cytoplasm at sub-cellular resolution in mouse cerebellum tissue[155]. With appropriate sample preparation and using 2,5-dihydroxyacetophenone as matrix, the transmission geometry principle was able to achieve a 1 µm laser spot diameter on target with a minimal raster step size of 2.5 µm. This approach allowed to produce mass spectrometry images of proteins acquired in a step raster mode at 5 pixels/s and in a continuous raster mode at 40 pixels/s[156], which is much faster than the 0.5-2 pixel/s acquisition of common QTOF and Orbitrap instruments. Increasing acquisition speed has the advantage that data is acquired within a reasonable time frame, which prevents molecular alteration of tissue in time from the beginning to the end of the MSI process. Zavalin *et al.*[157] developed a "laser beam filtration" approach, using lenses and a 25 µm ceramic spatial filter (pinhole) to remove the satellite secondary laser beam energy maxima resulting in a well-defined 5 µm diameter laser spot. The images generated from a mouse cerebellum showed clearly distinguishable cellular forms such as the Purkinje layer, dendrites, and axon fibers. Spengler's group introduced a Scanning Microprobe Matrix Assisted

Laser Desorption/Ionization (SMALDI)-MSI method, which features the possibility to investigate and visualize the spatial distribution of analytes including peptides such as bradykinin and angiotensin II in samples with sub-cellular resolution (0.5-10 µm) in pine tree roots[107,158].

Spatial resolution MSI of proteins from tissue sections can also be improved with specific sample preparation techniques or with dedicated data processing. Caprioli *et al.* have developed an approach to image proteins by blotting the tissue sections on a specially prepared target containing an adsorbent material[80]. Peptides and small proteins bind to the C_{18} material and create a positive imprint of the tissue, which can then be imaged by the mass spectrometer. The imprinted tissue material prevents any further delocalization of proteins and enables washing away interfering compounds such as lipids and salts. This approach has been applied to map proteins from the rat pituitary gland with a spatial resolution of ~25 µm. Integration of a coaxial laser illumination ion source into a MALDI-TOF-MS instrument allowed visualization of proteins of a molecular mass up to 27 kDa using this approach. In another study, two highly expressed secretory epididymal proteins in a mouse caudal epididymis tissue section were visualized, with a spatial resolution below 10 µm[92].

Low spatial resolution MSI data can be combined with high-resolution spatial microscopic images using multivariate regression called image fusion approach. Image fusion enables to predict distribution of MSI data at the spatial resolution of the H&E image. The resulting images combine the advantages of both technologies, enabling prediction of a molecular distribution both at high spatial resolution and maintaining the high chemical specificity of MSI data. For example, an ion image of *m/z* 778.5 (identified as a lipid) measured in mouse brain at 100 µm spatial resolution, can be extrapolated for 10 µm spatial resolution using fusion with H&E microscopy image measured from the same tissue sample at 10 µm resolution. Another example describes the prediction accuracy of an ion image with *m/z* 10,516 Da corresponding to an unidentified protein measured in a mouse brain section at 100 µm resolution and fused with an H&E microscopic image resulting in a predicted image at 5 µm resolution. This approach has been successfully applied for various tissue types, target molecules and histological staining protocols at different resolution scales. In addition, this approach can generate ion image predictions using microscopic images at the nanometer range, below the resolution achievable with current MALDI MSI instrumentation[159]. However, it should be noted that the image fusion approach is a statistical procedure predicting distribution at higher spatial resolution than the actually acquired MSI data. Therefore, thorough assessment of the prediction accuracy should be applied for each specific location and *m/z* slice.

A study from Spraggings *et al.*[160] presents an ultra-high speed MALDI-TOF MS, which provides image acquisition rates >25 pixels/s with high spatial resolution of 30 (full tissue section) and 10 µm (only selected tissue areas due to time required to collect the data) and a high mass resolution MALDI

Fourier transform ion cyclotron resonance (FTICR) MS operated with 100 µm spatial resolution. These novel instruments improve protein image acquisition rates by a factor of 10, can provide MALDI MSI data at 10 µm spatial resolution with good sensitivity, and isotopically resolve proteins up to 20 kDa. The data from these two instruments on the same tissue section could be combined e.g. with interpolation similar to the image fusion approaches resulting in high spatial resolution and high mass accuracy MSI data.

2.1.3 Identification of intact proteins in MSI

Intact proteins can be fragmented in the gas phase outside or inside the mass spectrometer through various mechanisms[161], such as MALDI in-source decay (ISD), collision-induced dissociation (CID), infrared multiphoton dissociation (IRMPD), electron capture dissociation (ECD), ETD, ultraviolet photodissociation (UVPD) and laser-induced dissociation (LID). Among these, MALDI ISD[162–164], where the fragmentation occurs in the MALDI ion source is the most widely used approach[80,76,165]. ISD has proven to be an efficient method for the N- and C-terminal sequencing of proteins in tissue sections. In ISD, proteins are cleaved at the N-C_α bond of the peptide backbone at high laser fluence (radiant exposure expressing the amount of energy received per unit of surface area) in the hot MALDI plume, giving principally c-and z-type protein fragments[166]. As early as 2001, Chaurand *et al.* applied ISD-MSI in the characterization of spermine-binding protein (SBP) in mouse prostate lobes with respect to sequence variants and PTMs and the localization of this protein[167]. The main advantage of ISD is that there is no mass limitation since fragmentation occurs prior to ion acceleration. However, ISD suffers from the major drawback of lack of precursor ion selection, which leads to a complicated mass spectrum if more than one protein is present at the laser shot position, which is generally the case in MSI of tissue section. In addition, many c- or z-fragment ions below 1000 Da are often difficult to assign due to the presence of matrix adduct peaks, making the identification of the sequence part close to the protein termini challenging. ISD-MSI require multiple laser shots in the same spot ablating all available proteins to gain the highest signal, which is a time-consuming task.

To circumvent this issue, a "pseudo-MS^3" approach, also known as "T^3-sequencing", has been developed to improve MALDI-ISD in proteins[168,169]. In this approach, the fragments produced by ISD are further isolated and fragmented with a classical tandem MS/MS approach in QTOF or MALDI-TOF/TOF instruments. The T^3-sequencing method with specific MALDI matrices, such as 2,5-dihydroxybenzoic acid or 1,5-diaminonaphthalene, has been applied to identify proteins such as myelin basic protein and crystallins in the tissue slices of mouse brain and porcine eye lens respectively[163]. The efficacy of MALDI-ISD-MSI to simultaneously identify the protein and determine its localization has been demonstrated in another study using tissue sections of porcine eye

lens. In this study a new bioinformatics pipeline was presented for processing MALDI-ISD-MSI data to identify proteins based on spectra containing high numbers of correlated fragments that are likely to be part of the same protein. This approach allows to determine the lateral spatial distribution of identified proteins as well[170]. Pauw and coworkers recently presented a high-resolution MALDI-ISD-FTICR method to identify a set of selected protein markers on histological slices simultaneously with minimal sample pretreatment[171]. In this method, known protein markers are spotted next to the tissue of interest and the whole MALDI plate is coated with 1,5-diaminonaphthalene matrix. The latter promotes MALDI ISD, providing large amino acid sequence tags. Comparative analysis of ISD fragments between the reference spots and the specimen in imaging mode allows for unambiguous identification of protein markers while preserving full spatial resolution, as well as the N- and C-terminal sequencing of proteins present in tissue sections. This was demonstrated with the distribution of myelin basic protein (MBP) from mouse brain and human neutrophil peptide 1 (HNP-1) in human liver sections containing metastasis from colorectal cancer.

Another approach to identify proteins uses fragmentation methods in mass spectrometers applied in "top-down" protein analysis such as ETD, ECD, or UVPD[172–175]. These might be applicable to top-down identification approaches in MSI, although the speed and sensitivity are currently not yet compatible with MSI. Even with these novel achievements, the detection of signals from intact proteins will still remain much easier than performing accurate identification, which will result in the fact that the majority of the protein signals in MSI remains unidentified.

2.2 Mass spectrometry imaging of proteins after *in situ* digestion

Another strategy used in MSI for protein imaging is *in situ* digestion prior to MALDI MSI analysis, which can be used to identify proteins and to determine protein distribution using surrogate proteotypic peptides. The method retrieves protein distributions in tissue sections using the corresponding proteotypic peptides after enzymatic digestion, most of the time using trypsin. Proteotypic peptides are those peptides that uniquely identify a protein and are used in bottom-up targeted and untargeted proteomics workflows to identify and quantify proteins with a (tandem) mass spectrometer[176]. In fact, peptides are smaller and, due to their better fragmentation, are easier to be identified by tandem mass spectrometry. Additionally, peptide fragments are easier to obtain than intact proteins from FFPE tissue. Therefore *in situ* digestion analysis is the method of choice for this sample type, which is more abundantly available in hospital biobanks compared to fresh frozen tissue samples. With this technique, Caprioli and coworkers described on-tissue identification of proteins in spatially discrete regions using tryptic digestion followed by MALDI MSI with (TOF-TOF) MS/MS analysis[177]. The procedure in this study identified several proteins in the coronal sections of a rat brain including higher molecular weight proteins, such as actin (41 kDa), tubulin (55 kDa), and

synapsin-1 (74 kDa). Ronci and Voelcker applied on-tissue trypsin digestion to analyze the freshly excised human lens capsule by MALDI MSI. This work demonstrated that the distribution of proteins can be determined from this highly compact connective tissue having no evident histo-morphological characteristics. Furthermore, the study shows a high repeatability of the digestion protocol on four different human lens capsule specimens by evaluating the distribution of the same set of peptides[178]. Recently, Diehl *et al.* optimized the *in situ* imaging of protein distribution after protease digestion with MALDI MSI using cryoconserved and FFPE rat brain tissue by applying different digestion times, types of matrix, and proteases[179]. The conclusion of this study was that the digestion time does not play an important role for the quality of MSI images, while trypsin provided the highest number of peptide signals corresponding to anatomical regions.

Ion mobility separation (IMS) combined with MSI has emerged as a powerful technique to improve specific detection of isobaric peptides with different molecular shape[25,180–182]. For example, Clench and coworkers successfully performed IMS-MSI to localize and identify peptides of the glucose-regulated protein 78 kDa (Grp78), which is known as a tumor biomarker, directly from FFPE pancreatic tumor tissue sections. Grp78 was found to be mainly located in tumor regions using MALDI-IMS-MSI[181]. In this procedure IMS separated isobaric peptides, which facilitated their identification following fragmentation, obtaining a cleaner image with less interferences for a particular peptide. Stauber *et al.* applied enzymatic digestion protocols for MALDI-IMS-MSI with high sensitivity localization and identification of proteins from FFPE and frozen tissues obtained from rat brain[182]. This study showed that isobaric peptides can be separated, which improves ion image specificity and improves identification accuracy of fragmented peptides.

Schober *et al.* presented a method for imaging tryptic peptides[183] in which MALDI MSI experiments were complemented by off-line liquid chromatography coupled to electrospray ionization tandem mass spectrometry (LC-ESI-MS/MS) analysis on an FT-ICR mass spectrometer to increase the number of identified peptides and proteins. Comparative results were obtained by analyzing two adjacent mouse brain sections in parallel. The first section was spotted with trypsin and analyzed by MALDI MSI. On-tissue MS/MS experiments of this section resulted in the identification of only 14 peptides (originating from 4 proteins). The second tissue section was homogenized, fractionated by ultracentrifugation and digested with trypsin prior to LC-ESI-MS/MS analysis. The number of identified peptides increased to 153 (corresponding to 106 proteins) by matching imaged mass peaks to peptides which were identified in these LC/ESI-MS/MS experiments. This identification difference can be explained that selected precursor ion windows in direct fragmentation of peptides from tissue include matrix and other interference which results in noisier spectra compared to LC-MS/MS analysis where these interferences are not present.

The group of McDonnell reported a comprehensive study of the mouse brain proteome from mouse brain slices with MSI using multiple proteases such as trypsin, Lys-C, Lys-N, Arg-C, and a mixture of trypsin and Lys-C[184]. This study combined identification of peptides and proteins from tissue using bottom-up LC-ESI-MS/MS and linked the obtained identifications using accurate mass with non-fragmented MSI data. In the LC-ESI-MS/MS data 5337 peptides were identified using complementary proteases, corresponding to 1198 proteins. 630 of these peptides, corresponding to 280 proteins, could be assigned to peaks in MSI data sets and used to determine the parent protein distribution in tissue. Gene ontology and pathway analyses revealed that many of the proteins are involved in neuro-degenerative disorders, such as Alzheimer's, Parkinson's, and Huntington's disease[184], which highlights the potential application of the technique in the future for diagnosis and pathology purposes.

Many approaches have been developed to improve protein identification performance in MALDI MSI after enzymatic digestion. For example, Franck *et al.* developed an N-terminal chemical derivatization strategy using 4-sulphophenyl isothiocyanate (4-SPITC), 3-sulfobenzoic acid (3-SBA) and N-succinimidyloxycarbonylmethyl-tris(2,4,6-trimethoxyphenyl)phosphonium bromide (TMPP) reagents, which improves *de novo* peptide identification performance[185]. The reagents added an additional positive or negative charge at the N-terminus of tryptic peptides, which provided more complete ion series upon fragmentation. From these reagents TMPP provided the best performance in terms of fragmentation efficiency of peptides from tissue. Clench's group used a recombinant protein termed "IMS-TAG" for MALDI-IMS-MSI[25]. The IMS-TAG recombinant proteins are engineered and used as a multi-protein standard. After trypsin digestion, this IMS-TAG protein yields – analogous to the QconCAT[186] approach – a range of peptides that can be used as internal standards to identify and quantify multiple proteins in a MALDI-IMS-MSI experiment. In this approach IMS is used to provide an additional selectivity to detect IMS-TAG derived standard peptides and to remove any potential interfering isobaric peptide signals. In this study, MALDI-IMS-MSI was used to measure the distribution of HSP90 and vimentin in FFPE EMT6 mouse tumor sections, as well as HSP90 and plectin in a fresh frozen mouse fibrosarcoma using extracted ion images at the corresponding *m/z* values and drift times from IMS-MSI data.

Performing accurate protein quantification in MSI is challenging since ion suppression due to other co-localized compounds can be strong and protein extraction and desorption can be partial in case of MSI of intact proteins. Trypsin digestion may alter quantification since this step creates a new ion suppression environment. The quantification performance can be made more accurate by using spiked stable isotope standards. For example, Porta *et al.* used stable isotope standards and performed quantification based on fragment ions obtained in SRM mode, which allowed to achieve a

quantification precision of 10-15%, which is sufficient to meet requirements of most bioanalysis guidelines[187]. A further finding of this work was that single pixel quantification is less accurate and at least the average of 4-5 pixels is required for accurate quantification of compounds in MSI data.

Komatsu *et al.* presented a feasibility study using a bismuth cluster ion (Bi_3^+) source with SIMS-TOF-MSI to determine protein distribution at the sub-cellular level combined with the ink-jet printing of trypsin. In this approach, a modified bubble jet printer (PIXUS 990i, Canon Inc.) was used to deposit trypsin and trifluoroacetic acid on a human serum albumin film layer. Protein images were obtained by visualizing the dot-patterned proteotypic peptide ions[188]. Nygren and Malmberg mapped tryptic fragments of thyroglobulin (660 kDa) in pig thyroid glands after trypsin digestion by SIMS-MSI using a Bi_3^+ primary ion source. In this study, trifluoroacetic acid in water was used to improve the ionization of the peptides, which resulted in a 3 μm spatial resolution MSI image showing a heterogeneous distribution of this protein in the thyroid follicle cells[40].

3 Targeted mass spectrometry imaging of protein in tissue using tag-mass probes

This section presents approaches to circumvent some of the shortcomings of MALDI MSI of proteins and peptides by not using matrix and detecting proteins with targeted indirect signals resulting from chemical derivatisation and immunochemistry recognition. Two major approaches are discussed in this section: the use of LA-ICP for detecting metals in proteins and the Tag-Mass approach.

LA-ICP MSI generates signals for targeted biomolecular imaging, which can be applied for MSI of proteins with high sensitivity and dynamic range, but at a relatively low spatial resolution (100-200 μm). For example, Seuma *et al.* studied the distribution of two breast cancer-associated proteins, MUC-1 and HER2 in tissue sections by measuring Au or Ag tagged antibodies, but although successful it was concluded that the image quality was inferior to microscopy[189]. Becker *et al.* demonstrated the potential of LA-ICP-MS to detect metalloproteins in protein bands or spots excised from 1D and 2D gel electropherograms. This method was then applied for sensitive and quantitative imaging of metals in brain sections, with detection limits for copper and zinc at the μg/g tissue level and below[190]. Giesen *et al.* applied LA-ICP-MSI for imaging metal-labelled antibodies to detect and quantify proteins directly in breast cancer and palatine tonsil tissue samples[191]. More recently, the same group developed this method further, and used 32 metal labeled antibodies to determine simultaneously 32 markers for protein and protein modification distribution in breast cancer tissue with laser ablation on a CyTOF instrument at subcellular resolution. The subcellular resolution at 1 μm enabled them to use this approach as mass spectrometry based cytometry i.e. to measure the concentration of these 32 protein markers in individual cells in tissue sections[192,193].

In 1998, a novel PC mass tag strategy for targeted detection of proteins has been suggested by Olejnik *et al.*[194]This strategy implements the targeted analysis of proteins by affinity labeling with an antibody (or another affinity agent) containing a PC mass tag and analyzing the labeled sample with LDI. The tag contains a PC-linker, linking the antibody to the mass tag, which is cleaved upon LDI, released into the gas phase, ionized and sampled into the mass spectrometer without the requirement to apply matrix for the analysis. Due to the absence of matrix, spatial resolution is not limited by the size of the analyte-matrix co-crystal and sensitivity is improved because detection of the released mass-tag reporter fragment ion does not interfere with matrix cluster ions. In the absence of matrix, the spatial distribution of LDI image is determined by the beam diameter of the applied laser. The PC-linker is cleaved with high yield under the near-UV laser pulses commonly used in MALDI-MS instruments. With a well-designed PC-linker and mass tag, this strategy has the ability to detect non-ionizing compounds and offers high selectivity and sensitivity for target proteins. Furthermore, coupling multiple PC-linked reporter mass tags to one affinity compound enhances the sensitivity of detection by increasing the MS signal[195].

Although MALDI MSI has a much lower lateral resolution than classical optical microscopy (<< 1 µm for example by using fluorescently labeled proteins), MS is both a sensitive method and allows for the simultaneous (mulitplexed) detection of hundreds to thousands of compounds. For fluorescence, only a restricted number of fluorophores are available, whereas the number of mass tags is only limited by the number of fragment ions that a mass analyzer can distinguish, which is *a priori* almost unlimited. Therefore, the mass tag method is a promising matrix-free strategy, which has a high multiplexing capacity, and the detection and localization of proteins in tissue sections with high specificity and sensitivity allowing to detect proteins larger than 30 kDa. A limitation is the availability of separate specific affinity reagents with unique mass tags for each protein to be measured and the specificity of the affinity tag.

In the literature, two types of photolinkers and reporter fragments (mass tags) have been reported, which have been developed by two different research teams. The group of Fournier described a targeted PC-linker strategy termed Tag-Mass based on the photocleavable linker 4-[4-[1-(Fmoc-amino)ethyl]-2-methoxy-5-nitrophenoxy]butanoic acid coupled to a peptide such as bradykinin as the mass tag. To study the possibility of using photocleavage under multiplex analysis conditions, this group used a mixture of three photocleavable-tagged oligonucleotide probes corresponding to three different 20-mer oligonucleotides recognizing particular mRNA (**Figure 4**)[22]. Although 100% photocleavage yield was not achieved using MALDI, the MS spectra showed the expected *m/z* of the mass tag demonstrating efficient photocleavage by laser irradiation. To increase the sensitivity, the group designed a new photocleavable linker/tag system by replacing the disulfide bridge with a

maleimide group for binding the peptide serving as mass tag to the photocleavable linker. This concept was applied to obtain specific images of proteins using tagged secondary antibodies. The results showed that MALDI appears to have a better sensitivity than the optical fluorescence images obtained from the same tissue section.

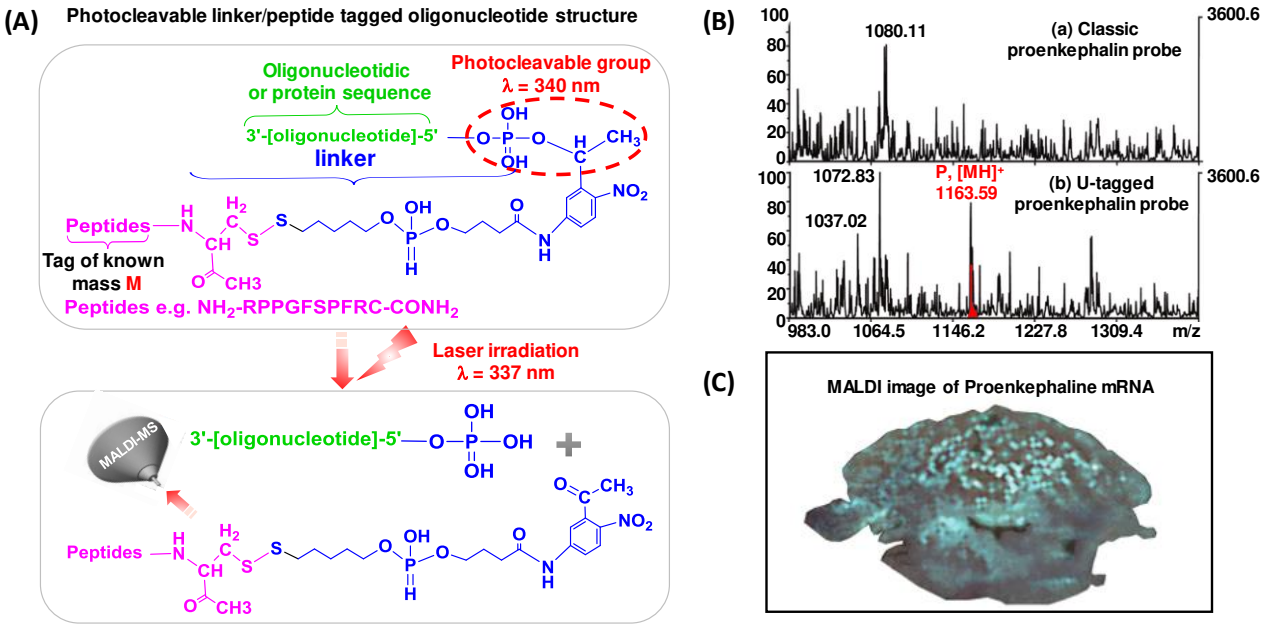

Figure 4. Structure of a photocleavable linker/tag system conjugated to an oligonucleotide/protein moiety and the reporter mass tag released via photocleavage as a result of irradiation by the UV laser (A). MALDI spectra of the untagged proenkephalin probe (upper plot) and the Uracil-tagged (U-tagged) proenkephalin probe (B) showing the peak highlighted in red corresponding to the applied mass tag in rat brain. Ion distribution image of the mass tag corresponding to the proenkephalin mRNA distribution. Adapted with permission from Lemaire *et al.* [22]. Copyright (2007) American Chemical Society.

The Tag-Mass strategy has been extended to different types of targeting compounds including secondary and primary antibodies, lectins and aptamers, which can be used to selectively obtain images of specific protein antigens, glycosylated proteins and drugs, respectively[24]. It can be combined with hybridization and affinity recognition techniques including *in situ* hybridization of mRNA (ISH) and immunohistochemistry (IHC)[22,24,196,197].

In 2007, Thiery *et al.*[198] reported a novel photocleavable mass-tag approach, where the released tag can be detected under LDI conditions and used for TAMSIM (**Figure 5**). TAMSIM is based on an N-hydroxysuccinimide (NHS) linker coupled to trityl reporters with a thioproprionate group, which provides low molecular weight fragments (500-600 Da) in LDI[198–200]. In this reagent, the trityl groups absorb UV light and form a resonance-stabilized carbocation, which results in cleavage of the C-S bond, and the release of the ionized mass-tag without the use of a matrix. This strategy was successfully applied to localize three different cancer markers on human tissue sections,

synaptophysin, protein S100 (PS100) and human melanosome (HMB45), that are normally below the detection threshold of untargeted MALDI MSI[198].

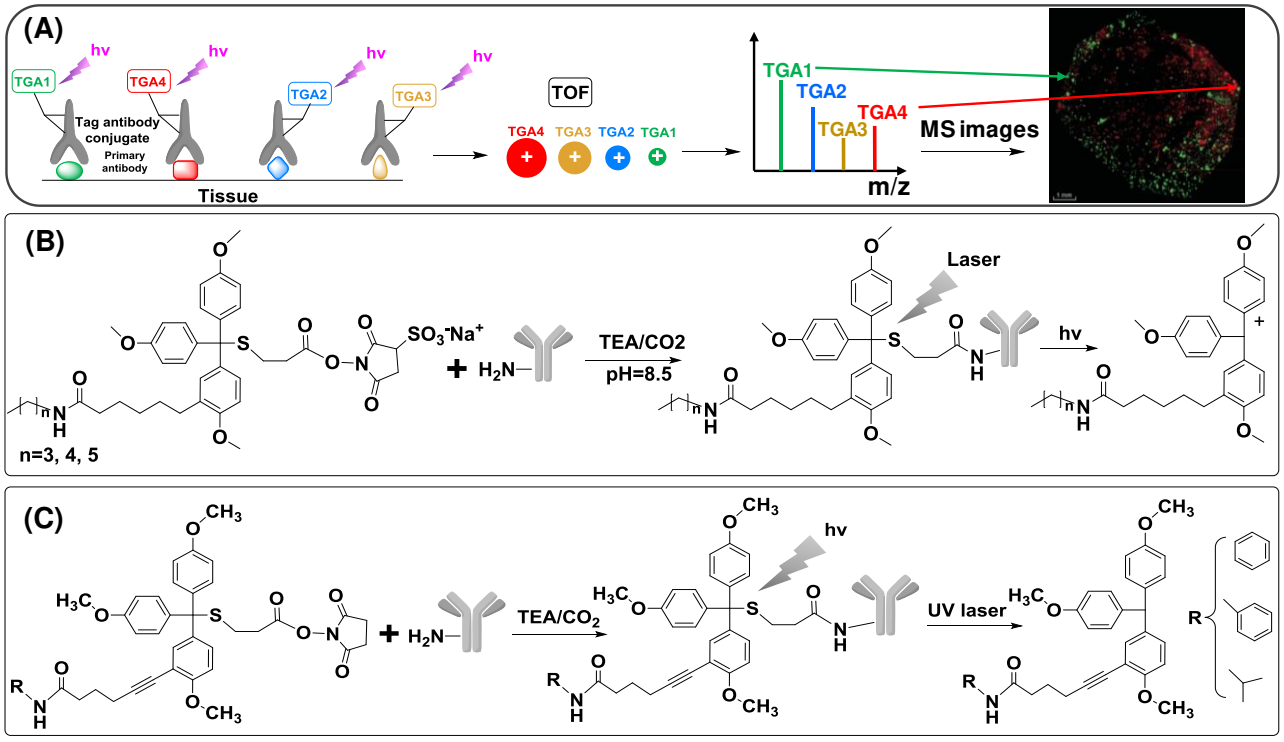

Figure 5. Concept of TAMSIM to measure protein spatial distributions in tissue sections with MSI using mass tag reporter ions conjugated via a photocleavable trityl group to antibodies. (A) Schematic representation of the mass-tag reporter ion released via photodissociation as a result of UV-laser irradiation upon cleavage of the trityl group coupled to the affinity tag. (B) Reaction steps of the conjugation of a mass tag reporter to an antibody via a photocleavable group and the release of the mass-tag reporter ion upon UV-laser irradiation. The photocleavable mass-tag reporter reagent contains an NHS ester as reactive group for covalent attachment to primary amino groups e.g. to the lysine residues of an antibody. In the ionization interface of the mass spectrometer the trityl groups absorb UV light resulting in the cleavage of the C-S bond and the release of the ionized mass-tag reporter ion. (C) Improved tags have the structure of alkyl or aromatic groups for mass tuning and exhibit higher stabilization of residue R on the tag. Plot (A) and (B) were adapted with permission from Thiery *et al.*[198] and (C) with permission from Thiery *et al*[201]. Copyright (2007 and 2008) American Chemical Society.

Subsequently, this approach was further improved by the same group (**Figure 5C**)[201]. In contrast to the previous version of TAMSIM, where the mass tags were coupled to secondary antibodies, the primary antibody is now directly conjugated with the affinity reagent and incubated with the tissue section. This improvement has the advantage to increase multiplexing as the approach is not limited by the number of species available for first and secondary antibody pair production. Additionally, new reporter tags were prepared, which differ from the previous tags at the level of the amide group. This new class of tags has conjugated alkynes or substituted aromatic groups, which allow for tuning the mass of the reporter tag and exhibit higher stabilization of the carbocation on the photocleavable reporter tag. These structural improvements provide more stable reagents, which facilitates handling

and sample preparation. The results showed that fewer fragments of the mass tag were observed in the gas phase, which leads to higher sensitivity. The method allowed to analyze FFPE and fresh frozen samples, with the latter having a lower number of artifact peaks in the mass spectra, as these mainly originated from paraffin in FFPE samples. This improved strategy was successfully applied to generate specific mass spectrometric images of three abundant proteins insulin, chromogranin A, and synaptophysin, and the less abundant proteins/peptides calcitonin and somastotatin localized in Langerhans islets[201].

Nevertheless, trityl-based PC-linkers still have several limitations. The highly hydrophobic character of the tagging reagent limits the number of PC-linker/mass tag reporters that can be conjugated to a single antibody, since it reduces the efficiency of the coupling reaction and the aqueous solubility of the resulting conjugates. To overcome this problem, Thiery *et al.* modified TAMSIM by using recombinant single chain variable fragments (scFv) originally designed from monoclonal IgG antibodies labeled with biotin.[195] The biotinylated scFv was coupled to avidin-holding multiple PC-reporter-tags to the biotin moiety to form an immune complex (IC). Essentially, the IC approach allowed the scFv to be linked to mass tags through biotin/avidin coupling and allowed to prepare the IC reagent in two steps, which was subsequently applied to the tissue section. The scFv linked to the reporter tag using this approach was used to specifically and simultaneously detect CYP1A1 and CYP1B1 in breast tumor tissue sections **(Figure 6)**. In 2015, Lorey *et al.*[23] presented a new signal detection method for antibody arrays using laser desorption/ionization-mass spectrometry (LDI-MS) based on small, photocleavable reporter molecules. In this work, signal amplification was achieved with a biotin labeled secondary antibody, where biotin is coupled to avidin holding several photocleavable mass-tags. Next, a highly sensitive sandwich assay is performed with immobilized primary antibody capturing prostate specific antigen (PSA) and the secondary antibody labeled with biotin/avidin/reporter-mass tag. This approach allowed to detect PSA in human plasma at clinically relevant concentrations ranging from 2 μg/mL to 200 pg/mL[23]. This assay has not been used for MSI yet, but it provides the option to determine the distribution of low abundant proteins in tissue sections. Yang *et al.*[202] developed an activity-based MSI approach using reporter mass tags, which provides high spatial resolution, and high sensitivity through the use of signal amplification chemistry and high target specificity **(Figure 7)**. In this approach, an activity-based probe (fluorophosphonate) that is specific for serine hydrolases is attached to a dendrimer through click chemistry containing more than 900 reporter tags leading to a signal amplification of nearly 3 orders of magnitude. On irradiation of the labeled tissue by the laser beam in a raster pattern, the mass tags are liberated and recorded by the mass spectrometer. Consequently, the ion image of the mass tag reveals the distribution of active serine hydrolases in rat brain and mouse embryo tissue sections. Hong *et al.* reported a mass tag-based MSI method that enables matrix-free MSI of protein biomarkers in FFPE tissues[203]. It involves

binding of the target protein with a primary antibody, followed by binding with a secondary antibody-enzyme conjugate. The substrate of the enzyme coupled to the secondary antibody is then added to the tissue section, and the enzyme converts the substrate to a product, which can be detected by LDI. The product is deposited at the location of the target protein by precipitation and the precipitates (e.g. diazonium salts) serve as reporter tags detected by mass spectrometry. The enzymes horseradish peroxidase and alkaline phosphatase and various substrates have been used to demonstrate the feasibility of this novel MSI method to image protein targets in FFPE tissue samples. The spatial resolution of this is only limited by the laser spot size of the commercially available instrument reaching limit of 10 µm without overlapping laser sampling area.

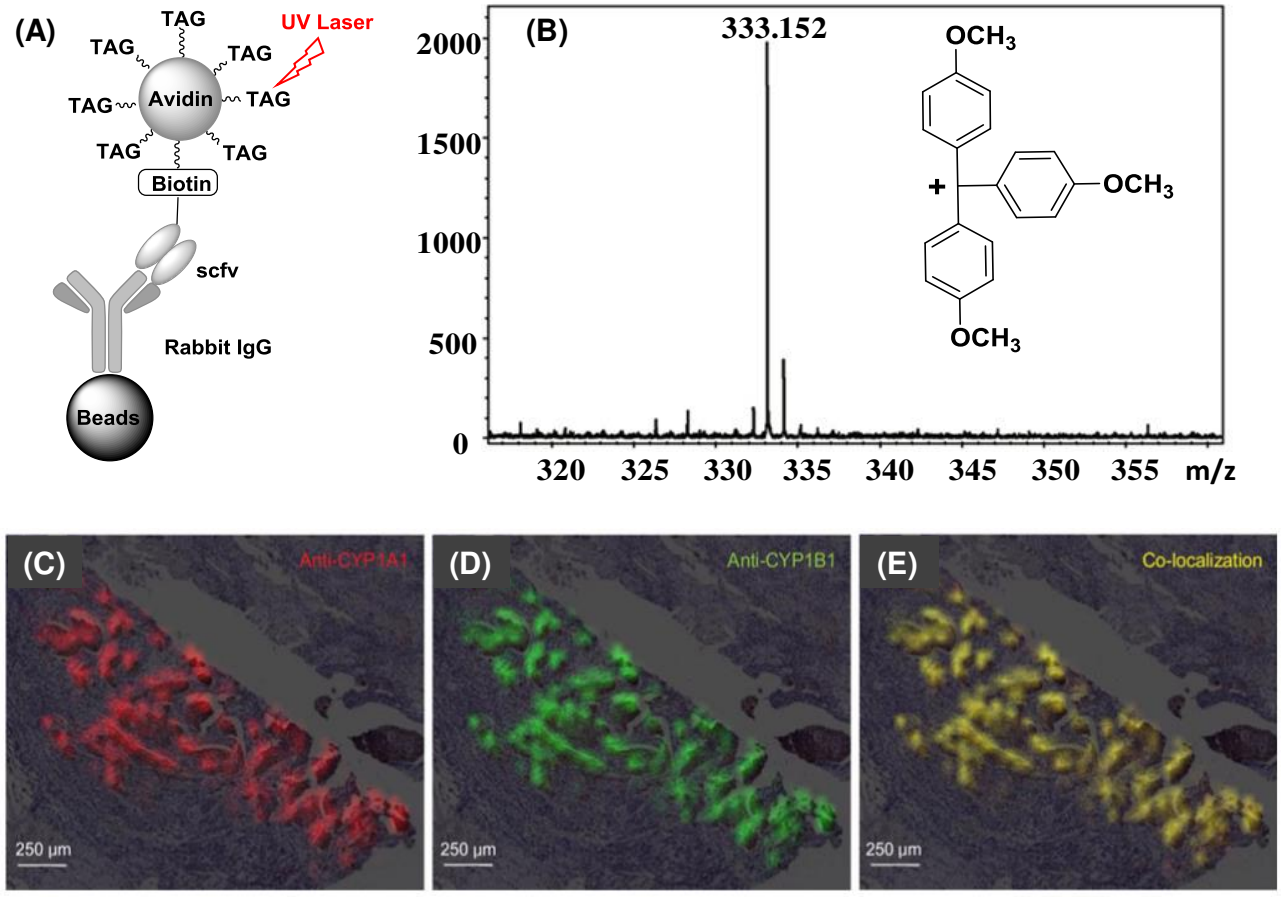

Figure 6. (A) Structure of the reagent used for targeted detection of reporter-tagged avidin bound to biotinylated A10B scFv on rabbit IgG coated beads used to optimize scfv-mass tag labeling. (B) Mass spectrum showing the released mass tag upon UV laser irradiation. (C-E) MS ion image of CYP1A1, CYP1B1 and both compounds on breast cancer tissue sections obtained by visualizing ion distribution of target compound specific reporter mass tag. The plot (E), which overlays the red and green colors of CYP1A1 and CYP1B1, respectively, shows that these two compounds are perfectly co-localized in the same tissue section. Adapted with permission from Thiery *et al.* [195]. Copyright (2012) American Society for Mass Spectrometry.

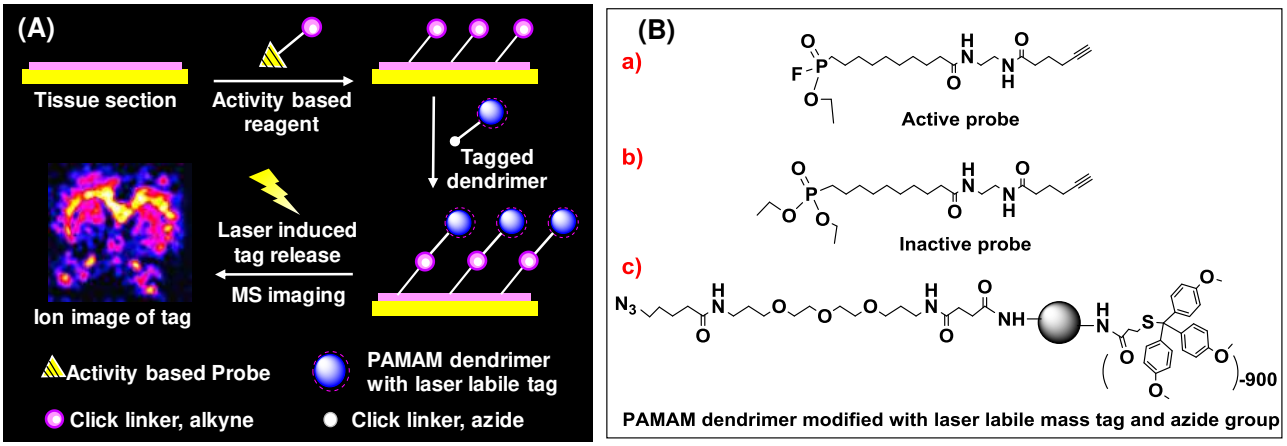

Figure 7. (A) MSI strategy using an activity-based probe conjugated to a PAMAM dendrimer modified with photocleavable mass tags. Structures of (B-a) active probe, (B-b) inactive probe, and (B-c) modified PAMAM dendrimer with the photocleavable mass tag and an azide group used to couple the PAMAM dendrimer with the alkyne group of the activity probe in tissue using click chemistry. Adapted with permission from Yang *et al.*[202]. Copyright (2012) American Chemical Society.

The PC-linker reporter tag strategy in MSI has significant advantages. The ability to detect a wide variety of proteins without the need of applying matrix helps to overcome previous limitations of MALDI MSI of intact proteins, i.e. low spatial resolution, restriction to the detection of high abundant and low molecular weight proteins with limited dynamic concentration range and incompatibility with FFPE tissues. The mass tag methods can be used to perform MSI on low-abundance proteins or to reveal the localization of active proteins in tissue. This approach can perform highly multiplexed analysis due to its ability to incorporate a large variety of reporter (mass) tags. However, it relies on the quality, cross-reactivity and reliability of the affinity tag (antibody, affimer or affinity probe) and provides a targeted and indirect signal of the proteins of interest, which alleviates to a certain extent the advantage of using mass spectrometry for detection.

4 Conclusions and Perspectives

The methods reviewed here emphasize the immense potential of MSI for studying the spatial distribution of proteins in tissue samples. Major challenges associated with sample preparation, data processing, and MS instrument design have been identified, particularly in order to simultaneously detect the distribution of large numbers of proteins with high spatial resolution and to extend the detected dynamic range with more accurate quantification. MSI of proteins is a rapidly developing field in analytical chemistry and recent developments such as novel ionization techniques, novel strategies for chemical labeling with photocleavable reporter (mass) tags, novel fragmentation approaches, and the improvements in mass spectrometry scanning speed are advancing all aspects of

this technology. For example, the mass tag-based LDI MSI approach, implemented as the Tag-Mass and TAMSIM methods, exhibits significant potential to achieve multiplexed imaging of proteins with high resolution in tissue sections with important applications in pathology laboratories as it can be used concurrent with immunohistochemistry staining. Recent advances in top-down mass spectrometry such as the enhanced transmission of high molecular mass protein ions[204,205] or the introduction of novel fragmentation approaches such as UVPD, which allow more complete fragmentation of intact proteins[173–175] confidently without the requirement for extensive cleanup, will further contribute to bringing protein MSI technology to maturation. Another trend holding potential improvement of protein MSI, is the combination of DESI and MALDI MSI, allowing to measure the lipid and protein distributions in subsequent analyses in the same tissue section[206]. In addition, MSI data can be integrated with spectroscopic images, including automatic annotation transfer of anatomic structures from microscopic images or from anatomical databases expanding the information content but also the dimensionality of the data.[207–209]. Combination of anatomical annotation, image fusion with bioinformatics solutions enabling to process and evaluate the large volume of MSI data in interactive way without loss of information would further improve the information that can be obtained from MSI studies.

All these technological advances will contribute to the full development of the MSI technology to profile protein distributions in tissues and will allow to broaden its scope in various fundamental and clinical applications, including new ways of pathological evaluation of tissue biopsies taken from patients to support diagnostics.

References

1 S. Rauser, S.-O. Deininger, D. Suckau, H. Höfler and A. Walch, *Expert Rev. Proteomics*, 2010, **7**, 927–41.

2 C. Schöne, H. Höfler and A. Walch, *Clin. Biochem.*, 2013, **46**, 539–545.

3 E. G. Solon, A. Schweitzer, M. Stoeckli and B. Prideaux, *AAPS J.*, 2010, **12**, 11–26.

4 G. Dimcevski, F. G. Erchinger, R. Havre and O. H. Gilja, *World J. Gastroenterol.*, 2013, **19**, 7247.

5 P. Flechsig, C. Walker, C. Kratochwil, L. König, A. Iagura, J. Moltz, T. Holland-Letz, H.-U. Kauczor, U. Haberkorn and F. L. Giesel, *Mol. Imaging Biol.*, 2017, 1–9.

6 M. F. Dumont, H. A. Hoffman, P. R. S. Yoon, L. S. Conklin, S. R. Saha, J. Paglione, R. W. Sze and R. Fernandes, *Bioconjug. Chem.*, 2014, **25**, 129–137.

7 R. Atreya, H. Neumann, C. Neufert, M. J. Waldner, U. Billmeier, Y. Zopf, M. Willma, C. App, T. Münster, H. Kessler, S. Maas, B. Gebhardt, R. Heimke-Brinck, E. Reuter, F. Dörje, T. T. Rau, W. Uter, T. D. Wang, R. Kiesslich, M. Vieth, E. Hannappel and M. F. Neurath, *Nat. Med.*, 2014, **20**, 313–318.

8 K. Cheng, S. R. Kothapalli, H. Liu, A. L. Koh, J. V. Jokerst, H. Jiang, M. Yang, J. Li, J. Levi, J. C. Wu, S. S. Gambhir and Z. Cheng, *J. Am. Chem. Soc.*, 2014, **136**, 3560–3571.

9 G. Lu and B. Fei, *J. Biomed. Opt.*, 2014, **19**, 010901.

10 W. R. W. Martin, *Mol. Imaging Biol.*, 2007, **9**, 196–203.

11 O. Golf, N. Strittmatter, T. Karancsi, S. D. Pringle, A. V. M. Speller, A. Mroz, J. M. Kinross, N. Abbassi-Ghadi, E. A. Jones and Z. Takats, *Anal. Chem.*, 2015, **87**, 2527–2534.

12 J. H. Gross, *Anal. Bioanal. Chem.*, 2014, **406**, 63–80.

13 R. M. Alberici, P. H. Vendramini and M. N. Eberlin, *Anal. Methods*, 2017, **9**, 5029–5036.

14 E. Esquenazi, C. Coates, L. Simmons, D. Gonzalez, W. H. Gerwick and P. C. Dorrestein, *Mol. Biosyst.*, 2008, **4**, 562–570.

15 Y. J. Lee, D. C. Perdian, Z. Song, E. S. Yeung and B. J. Nikolau, *Plant J.*, 2012, **70**, 81–95.

16 A. Römpp, S. Guenther, Y. Schober, O. Schulz, Z. Takats, W. Kummer and B. Spengler, *Angew. Chemie - Int. Ed.*, 2010, **49**, 3834–3838.

17 K. Huber, A. Feuchtinger, D. M. Borgmann, Z. Li, M. Aichler, S. M. Hauck, H. Zitzelsberger, M. Schwaiger, U. Keller and A. Walch, *Anal. Chem.*, 2014, **86**, 10568–10575.

18 R. Vismeh, D. J. Waldon, Y. Teffera and Z. Zhao, *Anal. Chem.*, 2012, **84**, 5439–5445.

19 M. R. Groseclose and S. Castellino, *Anal. Chem.*, 2013, **85**, 10099–10106.

20 J. G. Swales, J. W. Tucker, N. Strittmatter, A. Nilsson, D. Cobice, M. R. Clench, C. L. Mackay, P. E. Andren, Z. Takáts, P. J. H. Webborn and R. J. A. Goodwin, *Anal. Chem.*, 2014, **86**, 8473–80.

21 S. J. B. Dunham, J. F. Ellis, B. Li and J. V. Sweedler, *Acc. Chem. Res.*, 2017, **50**, 96–104.

22 R. Lemaire, J. Stauber, M. Wisztorski, C. Van Camp, A. Desmons, M. Deschamps, G. Proess, I. Rudlof, A. S. Woods, R. Day, M. Salzet and I. Fournier, *J. Proteome Res.*, 2007, **13**, 2057–2067.

23 M. Lorey, B. Adler, H. Yan, R. Soliymani, S. Ekström, J. Yli-Kauhaluoma, T. Laurell and M. Baumann, *Anal. Chem.*, 2015, **87**, 5255–5262.

24 J. Stauber, M. El Ayed, M. Wisztorski, M. Salzet and I. Fournier, Humana Press, Totowa, NJ, 2010, pp. 339–361.

25 L. M. Cole, K. Mahmoud, S. Haywood-Small, G. M. Tozer, D. P. Smith and M. R. Clench, *Rapid Commun. Mass Spectrom.*, 2013, **27**, 2355–2362.

26 K. Dreisewerd, *Anal. Bioanal. Chem.*, 2014, **406**, 2261–2278.

27 B. Balluff, C. Schöne, H. Höfler and A. Walch, *Histochem. Cell Biol.*, 2011, **136**, 227–44.

28 B. K. Kaletaş, I. M. Van Der Wiel, J. Stauber, L. J. Dekker, C. Güzel, J. M. Kros, T. M. Luider and R. M. A. Heeren, *Proteomics*, 2009, 9, 2622–2633.

29 R. J. A. Goodwin, *J. Proteomics*, 2012, **75**, 4893–4911.

30 M.-C. Djidja, E. Claude, P. Scriven, D. W. Allen, V. A. Carolan and M. R. Clench, *Biochim. Biophys. Acta - Proteins Proteomics*, 2017, **1865**, 901–906.

31 S. Ongay, M. Langelaar-Makkinje, M. P. Stoop, N. Liu, H. Overkleeft, T. M. Luider, G. M. M. Groothuis and R. Bischoff, *ChemBioChem*, 2018, **19**, 736–743.

32 R. J. A. Goodwin, S. R. Pennington and A. R. Pitt, *Proteomics*, 2008, **8**, 3785–3800.

33 P. Chaurand, J. L. Norris, D. S. Cornett, J. A. Mobley and R. M. Caprioli, *J. Proteome Res.*, 2006, 5, 2889–2900.

34 R. J. A. Goodwin, S. R. Pennington and A. R. Pitt, *Proteomics*, 2008, 8, 3785–3800.

35 W. Bouschen and B. Spengler, *Int. J. Mass Spectrom.*, 2007, **266**, 129–137.

36 T. W. Jaskolla, M. Karas, U. Roth, K. Steinert, C. Menzel and K. Reihs, *J. Am. Soc. Mass Spectrom.*, 2009, **20**, 1104–1114.

37 P. Chaurand, S. A. Schwartz, D. Billheimer, B. J. Xu, A. Crecelius and R. M. Caprioli, *Anal. Chem.*, 2004, **76**, 1145–1155.

38 H. R. Aerni, D. S. Cornett and R. M. Caprioli, *Anal. Chem.*, 2006, **78**, 827–834.

39 H. Liebl, *J. Appl. Phys.*, 1967, **38**, 5277–5283.

40 H. Nygren and P. Malmberg, *Proteomics*, 2010, **10**, 1694–1698.

41 E. de. Hoffmann and V. Stroobant, *Mass spectrometry : principles and applications*, J. Wiley, 2007.

42 J. J. D. Fitzgerald, P. Kunnath and A. V Walker, *Technology*, 2010, **82**, 4413–4419.

43 J. Xu, S. Ostrowski, C. Szakal, A. G. Ewing and N. Winograd, in *Applied Surface Science*, 2004, vol. 231–232, pp. 159–163.

44 R. M. A. Heeren, L. A. McDonnell, E. Amstalden, S. L. Luxembourg, A. F. M. Altelaar and S. R. Piersma, *Appl. Surf. Sci.*, 2006, **252**, 6827–6835.

45 S. G. Boxer, M. L. Kraft and P. K. Weber, *Annu. Rev. Biophys.*, 2009, **38**, 53–74.

46 F. Kollmer, W. Paul, M. Krehl and E. Niehuis, in *Surface and Interface Analysis*, 2013, vol. 45, pp. 312–314.

47 N. Winograd, *Anal. Chem.*, 2015, 87, 328–333.

48 J. S. Fletcher and J. C. Vickerman, *Anal. Bioanal. Chem.*, 2010, **396**, 85–104.

49 J. S. Fletcher, J. C. Vickerman and N. Winograd, *Curr. Opin. Chem. Biol.*, 2011, 15, 733–740.

50 R. Hill, P. Blenkinsopp, S. Thompson, J. Vickerman and J. S. Fletcher, in *Surface and Interface Analysis*, 2011, vol. 43, pp. 506–509.

51 J. S. Fletcher, N. P. Lockyer, S. Vaidyanathan and J. C. Vickerman, *Anal. Chem.*, 2007, **79**, 2199–2206.

52 J. S. Fletcher, N. P. Lockyer and J. C. Vickerman, *Mass Spectrom. Rev.*, 2011, **30**, 142–174.

53 E. J. Lanni, S. S. Rubakhin and J. V. Sweedler, *J. Proteomics*, 2012, **75**, 5036–5051.

54 S. Solé-Domènech, P. Sjövall, V. Vukojević, R. Fernando, A. Codita, S. Salve, N. Bogdanović, A. H. Mohammed, P. Hammarström, K. P. R. Nilsson, F. M. Laferla, S. Jacob, P. O. Berggren, L. Giménez-Llort, M. Schalling, L. Terenius and B. Johansson, *Acta Neuropathol.*, 2013, **125**, 145–157.

55 J. S. Fletcher, *Analyst*, 2009, **134**, 2204.

56 J. S. Fletcher, S. Rabbani, A. Henderson, P. Blenkinsopp, S. P. Thompson, N. P. Lockyer and J. C. Vickerman, *Anal. Chem.*, 2008, **80**, 9058–9064.

57 E. J. Lanni, S. J. B. Dunham, P. Nemes, S. S. Rubakhin and J. V. Sweedler, *J. Am. Soc. Mass Spectrom.*, 2014, **25**, 1897–1907.

58 K. Chughtai and R. M. A. Heeren, *Chem. Rev.*, 2010, **110**, 3237–3277.

59 Z. Takáts, J. M. Wiseman, B. Gologan and R. G. Cooks, *Science (80-.).*, 2004, **306**, 471–473.

60 J. M. Wiseman, D. R. Ifa, Q. Song and R. G. Cooks, *Angew. Chemie - Int. Ed.*, 2006, **45**, 7188–7192.

61 M. Nefliu, J. N. Smith, A. Venter and R. G. Cooks, *J. Am. Soc. Mass Spectrom.*, 2008, **19**, 420–427.

62 C. Wu, D. R. Ifa, N. E. Manicke and R. G. Cooks, *Analyst*, 2010, **135**, 28–32.

63 T. Müller, S. Oradu, D. R. Ifa, R. G. Cooks and B. Kräutler, *Anal. Chem.*, 2011, **83**, 5754–5761.

64 L. S. Eberlin, C. R. Ferreira, A. L. Dill, D. R. Ifa and R. G. Cooks, *Biochim. Biophys. Acta - Mol. Cell Biol. Lipids*, 2011, **1811**, 946–960.

65 S. R. Ellis, C. Wu, J. M. Deeley, X. Zhu, R. J. W. Truscott, M. in het Panhuis, R. G. Cooks, T. W. Mitchell and S. J. Blanksby, *J. Am. Soc. Mass Spectrom.*, 2010, **21**, 2095–2104.

66 J. Thunig, S. H. Hansen and C. Janfelt, *Anal. Chem. (Washington, DC, United States)*, 2011, **83**, 3256–3259.

67 J. Watrous, N. Hendricks, M. Meehan and P. C. Dorrestein, *Anal. Chem.*, 2010, **82**, 1598–1600.

68 Z. Takáts, J. M. Wiseman and R. G. Cooks, *J. Mass Spectrom.*, 2005, 40, 1261–1275.

69 C. Janfelt and A. W. Nørgaard, *J. Am. Soc. Mass Spectrom.*, 2012, **23**, 1670–1678.

70 M. Girod, Y. Shi, J. X. Cheng and R. G. Cooks, *Anal. Chem.*, 2011, **83**, 207–215.

71 V. Kertesz and G. J. Van Berkel, *Rapid Commun. Mass Spectrom.*, 2008, **22**, 2639–2644.

72 W. Rao, D. J. Scurr, J. Burston, M. R. Alexander and D. a Barrett, *Analyst*, 2012, **137**, 3946.

73 K. Y. Garza, C. L. Feider, D. R. Klein, J. A. Rosenberg, J. S. Brodbelt and L. S. Eberlin, *Anal. Chem.*, 2018, **90**, 7785–7789.

74 P. Nemes and A. Vertes, *Anal. Chem.*, 2007, **79**, 8098–8106.

75 J. Zou, F. Talbot, A. Tata, L. Ermini, K. Franjic, M. Ventura, J. Zheng, H. Ginsberg, M. Post, D. R. Ifa, D. Jaffray, R. J. D. Miller and A. Zarrine-Afsar, *Anal. Chem.*, 2015, **87**, 12071–12079.

76 M. Stoeckli, P. Chaurand, D. E. Hallahan and R. M. Caprioli, *Nat. Med.*, 2001, **7**, 493–496.

77 M. Karas and F. Hillenkamp, *Anal. Chem.*, 1988, 60, 2299–2301.

78 R. Limberg and S. D. Gmbh, 1988, **2301**, 2299–2301.

79 A. Römpp and B. Spengler, *Histochem. Cell Biol.*, 2013, **139**, 759–783.

80 R. M. Caprioli, T. B. Farmer and J. Gile, *Anal. Chem.*, 1997, **69**, 4751–60.

81 P. Chaurand, S. A. Schwartz and R. M. Caprioli, *Curr. Opin. Chem. Biol.*, 2002, **6**, 676–681.

82 N. Verbeeck, J. Yang, B. De Moor, R. M. Caprioli, E. Waelkens and R. Van de Plas, *Anal. Chem.*, 2014, **86**, 8974–82.

83 M. Karas and R. Kr??ger, *Chem. Rev.*, 2003, **103**, 427–439.

84 J. Yang and R. M. Caprioli, *Anal. Chem.*, 2011, **83**, 5728–5734.

85 S. R. Ellis, J. H. Jungmann, D. F. Smith, J. Soltwisch and R. M. a Heeren, *Angew. Chem. Int. Ed. Engl.*, 2013, **52**, 11261–4.

86 J. E. Yarnold, B. R. Hamilton, D. T. Welsh, G. F. Pool, D. J. Venter and A. R. Carroll, *Mol. Biosyst.*, 2012, **8**, 2249–59.

87 P. M. Angel, J. M. Spraggins, H. S. Baldwin and R. Caprioli, *Anal. Chem.*, 2012, **84**, 1557–1564.

88 M. Poetzsch, A. E. Steuer, A. T. Roemmelt, M. R. Baumgartner and T. Kraemer, *Anal. Chem.*, 2014, **86**, 11758–65.

89 X. C. Yu, O. V. Borisov, M. Alvarez, D. A. Michels, Y. J. Wang and V. Ling, *Anal. Chem.*, 2009, **81**, 9282–9290.

90 A. Römpp, S. Guenther, Z. Takats and B. Spengler, *Anal. Bioanal. Chem.*, 2011, **401**, 65–73.

91 C. Dai, L. H. Cazares, L. Wang, Y. Chu, S. L. Wang, D. a Troyer, O. J. Semmes, R. R. Drake and B. Wang, *Chem. Commun. (Camb).*, 2011, **47**, 10338–10340.

92 P. Chaurand, K. E. Schriver and R. M. Caprioli, *J. Mass Spectrom.*, 2007, **42**, 476–489.

93 Y. Li, B. Shrestha and A. Vertes, *Anal. Chem.*, 2008, **80**, 407–420.

94 Y. Li, B. Shrestha and A. Vertes, 2007, **79**, 523–532.

95 D. R. am Bhandari, M. Schott, A. Römpp, A. Vilcinskas and B. Spengler, *Anal. Bioanal. Chem.*, 2015, **407**, 2189–2201.

96 S. M. Khalil, A. Römpp, J. Pretzel, K. Becker and B. Spengler, *Anal. Chem.*, 2015, **87**, 11309–11316.

97 M. Kompauer, S. Heiles and B. Spengler, *Nat. Methods*, 2016, **14**, 90–96.

98 C. Keller, J. Maeda, D. Jayaraman, S. Chakraborty, M. R. Sussman, J. M. Harris, J.-M. Ané and L. Li, *Front. Plant Sci.*, 2018, **9**, 1238.

99 J. S. Sampson, A. M. Hawkridge and D. C. Muddiman, *J. Am. Soc. Mass Spectrom.*, 2006, **17**, 1712–1716.

100 J. S. Sampson and D. C. Muddiman, *Rapid Commun. Mass Spectrom.*, 2009, **23**, 1989–1992.

101 J. Sabine Becker, *J. Mass Spectrom.*, 2013, **48**, 255–268.

102 J. S. Becker, M. Zoriy, A. Matusch, B. Wu, D. Salber, C. Palm and J. S. Becker, *Mass Spectrom. Rev.*, 2010, **29**, 156–175.

103 I. Feldmann, C. U. Koehler, P. H. Roos and N. Jakubowski, *J. Anal. At. Spectrom.*, 2006, **21**, 1006.

104 F. Schueder, J. Lara-Gutiérrez, B. J. Beliveau, S. K. Saka, H. M. Sasaki, J. B. Woehrstein, M. T. Strauss, H. Grabmayr, P. Yin and R. Jungmann, *Nat. Commun.*, 2017, **8**, 2090.

105 J. R. Chirinos, D. D. Oropeza, J. J. Gonzalez, H. Hou, M. Morey, V. Zorba and R. E. Russo, *J. Anal. At. Spectrom.*, 2014, **29**, 1292–1298.

106 S. K. EDELMAN, *Echocardiography*, 1988, **5**, 269–272.

107 B. Spengler and M. Hubert, *J. Am. Soc. Mass Spectrom.*, 2002, **13**, 735–748.

108 D. Trede, S. Schiffler, M. Becker, S. Wirtz, K. Steinhorst, J. Strehlow, M. Aichler, J. H. Kobarg, J. Oetjen, A. Dyatlov, S. Heldmann, A. Walch, H. Thiele, P. Maass and T. Alexandrov, *Anal. Chem.*, 2012, **84**, 6079–6087.

109 M. Andersson, M. R. Groseclose, A. Y. Deutch and R. M. Caprioli, *Nat. Methods*, 2008, **5**, 101–108.

110 L. Morosi, S. Giordano, F. Falcetta, R. Frapolli, S. A. Licandro, C. Matteo, M. Zucchetti, P. Ubezio, E. Erba, S. Visentin, M. D'Incalci and E. Davoli, *Clin. Pharmacol. Ther.*, 2017, **102**, 748–751.

111 E. H. Seeley and R. M. Caprioli, *Anal. Chem.*, 2012, **84**, 2105–2110.

112 S. Giordano, L. Morosi, P. Veglianese, S. A. Licandro, R. Frapolli, M. Zucchetti, G. Cappelletti, L. Falciola, V. Pifferi, S. Visentin, M. D'Incalci and E. Davoli, *Sci. Rep.*, 2016, **6**, 37027.

113 D. Touboul and A. Brunelle, *Mass Spectrometry Imaging of Small Molecules*, Springer New York, New York, NY, 2015, vol. 1203.

114 G. Jacobs, *Prof. Surv. Mag.*

115 S. Keren, C. Zavaleta, Z. Cheng, A. de la Zerda, O. Gheysens and S. S. Gambhir, *Proc. Natl. Acad. Sci. U. S. A.*, 2008, **105**, 5844–9.

116 J. C. Jurchen, S. S. Rubakhin and J. V. Sweedler, *J. Am. Soc. Mass Spectrom.*, 2005, **16**, 1654–1659.

117 M. Nazari and D. C. Muddiman, *Anal. Bioanal. Chem.*, 2015, **407**, 2265–2271.

118 A. D. Palmer and T. Alexandrov, *Anal. Chem.*, 2015, **87**, 4055–4062.

119 D. Trede, S. Schi, M. Becker, S. Wirtz, K. Steinhorst, J. Strehlow, M. Aichler, J. H. Kobarg, J. Oetjen, A. Dyatlov, S. Heldmann, A. Walch, H. Thiele, P. Maass and T. Alexandrov, *Anal. Chem.*, 2012, **84**, 6079–6087.

120 A. Bouslimani, C. Porto, C. M. Rath, M. Wang, Y. Guo, A. Gonzalez, D. Berg-Lyon, G. Ackermann, G. J. Moeller Christensen, T. Nakatsuji, L. Zhang, A. W. Borkowski, M. J. Meehan, K. Dorrestein, R. L. Gallo, N. Bandeira, R. Knight, T. Alexandrov and P. C. Dorrestein, *Proc. Natl. Acad. Sci.*, 2015, **112**, E2120–E2129.

121 T. Alexandrov, *BMC Bioinformatics*, 2012, **13 Suppl 1**, S11.

122 E. E. Jones, C. Quiason, S. Dale and S. K. Shahidi-Latham, *J. Am. Soc. Mass Spectrom.*, 2017, **28**, 1709–1715.

123 F. Suits, T. E. Fehniger, Á. Végvári, G. Marko-Varga and P. Horvatovich, *Anal. Chem.*, 2013, **85**, 4398–4404.

124 T. E. Fehniger, F. Suits, Á. Végvári, P. Horvatovich, M. Foster and G. Marko-Varga, *Proteomics*, 2014, **14**, 862–871.

125 W. M. Abdelmoula, K. Škrášková, B. Balluff, R. J. Carreira, E. A. Tolner, B. P. F. Lelieveldt, L. Van Der Maaten, H. Morreau, A. M. J. M. Van Den Maagdenberg, R. M. A. Heeren, L. A. McDonnell and J.

Dijkstra, *Anal. Chem.*, 2014, **86**, 9204–9211.

126 L. A. McDonnell, A. Walch, M. Stoeckli and G. L. Corthals, *J. Proteome Res.*, 2014, **13**, 1138–1142.

127 T. Alexandrov, *BMC Bioinformatics*, 2012, **13 Suppl 1**, S11.

128 T. Schramm, A. Hester, I. Klinkert, J. P. Both, R. M. A. Heeren, A. Brunelle, O. Laprévote, N. Desbenoit, M. F. Robbe, M. Stoeckli, B. Spengler and A. Römpp, *J. Proteomics*, 2012, **75**, 5106–5110.

129 A. Römpp, T. Schramm, A. Hester, I. Klinkert, J.-P. Both, R. M. A. Heeren, M. Stöckli and B. Spengler, *Methods Mol. Biol.*, 2011, **696**, 205–24.

130 G. Mayer, L. Montecchi-Palazzi, D. Ovelleiro, A. R. Jones, P. A. Binz, E. W. Deutsch, M. Chambers, M. Kallhardt, F. Levander, J. Shofstahl, S. Orchard, J. A. Vizcaíno, H. Hermjakob, C. Stephan, H. E. Meyer and M. Eisenacher, *Database*, 2013, **2013**, bat009-bat009.

131 O. Jardin-Mathé, D. Bonnel, J. Franck, M. Wisztorski, E. Macagno, I. Fournier and M. Salzet, *J. Proteomics*, 2008, **71**, 332–345.

132 M. F. Robbe, J. P. Both, B. Prideaux, I. Klinkert, V. Picaudd, T. Schramm, A. Hester, V. Guevara, M. Stoeckli, A. Roempp, R. Heeren, B. Spengler, O. Gala and S. Haana, *Eur. J. Mass Spectrom.*, 2014, **20**, 351–360.

133 J. Oetjen, K. Veselkov, J. Watrous, J. S. McKenzie, M. Becker, L. Hauberg-Lotte, J. H. Kobarg, N. Strittmatter, A. K. Mróz, F. Hoffmann, D. Trede, A. Palmer, S. Schiffler, K. Steinhorst, M. Aichler, R. Goldin, O. Guntinas-Lichius, F. von Eggeling, H. Thiele, K. Maedler, A. Walch, P. Maass, P. C. Dorrestein, Z. Takats and T. Alexandrov, *Gigascience*, 2015, **4**, 20.

134 V. Delcourt, J. Franck, E. Leblanc, F. Narducci, Y.-M. Robin, J.-P. Gimeno, J. Quanico, M. Wisztorski, F. Kobeissy, J.-F. Jacques, X. Roucou, M. Salzet and I. Fournier, *EBioMedicine*, 2017, **21**, 55–64.

135 J. Sarsby, N. J. Martin, P. F. Lalor, J. Bunch and H. J. Cooper, *J. Am. Soc. Mass Spectrom.*, 2014, **25**, 1953–1961.

136 M. Lagarrigue, M. Becker, R. Lavigne, S.-O. Deininger, A. Walch, F. Aubry, D. Suckau and C. Pineau, *Mol. Cell. Proteomics*, 2011, **10**, M110.005991-M110.005991.

137 M. Ronci, S. Sharma, S. Martin, J. E. Craig and N. H. Voelcker, *J. Proteomics*, 2013, **82**, 27–34.

138 B. D. Leinweber, G. Tsaprailis, T. J. Monks and S. S. Lau, *J. Am. Soc. Mass Spectrom.*, 2009, **20**, 89–95.

139 A. C. Grey, P. Chaurand, R. M. Caprioli and K. L. Schey, *J. Proteome Res.*, 2009, **8**, 3278–3283.

140 J. Franck, R. Longuespée, M. Wisztorski, A. Van Remoortere, R. Van Zeijl, A. Deelder, M. Salzet, L. McDonnell and I. Fournier, *Med. Sci. Monit.*, 2010, **16**, BR293-9.

141 V. Mainini, G. Bovo, C. Chinello, E. Gianazza, M. Grasso, G. Cattoretti and F. Magni, *Mol. Biosyst.*, 2013, **9**, 1101.

142 D. C. Reiber, T. a Grover and R. S. Brown, *Anal. Chem.*, 1998, **70**, 673–683.

143 N. L. Kelleher, *Anal. Chem.*, 2004, **76**, 196 A-203 A.

144 R. Lemaire, A. Desmons, J. C. Tabet, R. Day, M. Salzet and I. Fournier, *J. Proteome Res.*, 2007, **6**, 1295–1305.

145 R. J. Rose, E. Damoc, E. Denisov, A. Makarov and A. J. R. Heck, *Nat. Methods*, 2012, **9**, 1084–1086.

146 A. van Remoortere, R. J. M. van Zeijl, N. van den Oever, J. Franck, R. Longuespée, M. Wisztorski, M. Salzet, A. M. Deelder, I. Fournier and L. A. McDonnell, *J. Am. Soc. Mass Spectrom.*, 2010, **21**, 1922–1929.

147 J. H. Jungmann, L. MacAleese, J. Visser, M. J. J. Vrakking and R. M. A. Heeren, *Anal. Chem.*, 2011, **83**, 7888–7894.

148 R. Knochenmuss and R. Zenobi, *Chem. Rev.*, 2003, **103**, 441–452.

149 K. Dreisewerd, M. Schürenberg, M. Karas and F. Hillenkamp, *Int. J. Mass Spectrom. Ion Process.*, 1995, **141**, 127–148.

150 R. Knochenmuss and L. V. Zhigilei, *Anal. Bioanal. Chem.*, 2012, **402**, 2511–2519.

151 R. Zenobi and R. Knochenmuss, 1999, 337–366.

152 M. Martin-Lorenzo, B. Balluff, A. Sanz-Maroto, R. J. M. van Zeijl, F. Vivanco, G. Alvarez-Llamas and L. A. McDonnell, *J. Proteomics*, 2014, **108**, 465–468.

153 F. Deutskens, J. Yang and R. M. Caprioli, *J. Mass Spectrom.*, 2011, **46**, 568–571.

154 Y. Schober, S. Guenther, B. Spengler and A. Römpp, *Anal. Chem.*, 2012, **84**, 6293–6297.

155 A. Zavalin, E. M. Todd, P. D. Rawhouser, J. Yang, J. L. Norris and R. M. Caprioli, *J. Mass Spectrom.*, 2012, **47**, 1473–1481.

156 A. Zavalin, J. Yang, K. Hayden, M. Vestal and R. M. Caprioli, *Anal. Bioanal. Chem.*, 2015, **407**, 2337–42.

157 A. Zavalin, J. Yang and R. Caprioli, *J. Am. Soc. Mass Spectrom.*, 2013, **24**, 1153–1156.

158 M. Koestler, D. Kirsch, A. Hester, A. Leisner, S. Guenther and B. Spengler, *Rapid Commun. Mass Spectrom.*, 2008, **22**, 3275–3285.

159 R. Van De Plas, J. Yang, J. Spraggins and R. M. Caprioli, *Nat. Methods*, 2015, **12**, 366–372.

160 J. M. Spraggins, D. G. Rizzo, J. L. Moore, M. J. Noto, E. P. Skaar and R. M. Caprioli, *Proteomics*, 2016, **16**, 1678–1689.

161 D. Calligaris, C. Villard and D. Lafitte, *J. Proteomics*, 2011, **74**, 920–934.

162 D. Bonnel, R. Longuespee, J. Franck, M. Roudbaraki, P. Gosset, R. Day, M. Salzet and I. Fournier, *Anal. Bioanal. Chem.*, 2011, **401**, 149–165.

163 D. Debois, V. Bertrand, L. Quinton, M. C. De Pauw-Gillet and E. De Pauw, *Anal. Chem.*, 2010, **82**, 4036–4045.

164 J. Hardouin, *Mass Spectrom. Rev.*, 2007, **26**, 672–82.

165 K. E. Burnum, S. L. Frappier and R. M. Caprioli, *Annu. Rev. Anal. Chem. (Palo Alto. Calif).*, 2008, **1**, 689–705.

166 M. Takayama, *J. Mass Spectrom. Soc. Jpn.*, 2002, **50**, 304–310.

167 P. Chaurand, B. B. DaGue, S. Ma, S. Kasper and R. M. Caprioli, 2001, **40**, 9725–9733.

168 C. S. Raska, C. E. Parker, C. Huang, J. Han, G. L. Glish, M. Pope and C. H. Borchers, *J. Am. Soc. Mass Spectrom.*, 2002, **13**, 1034–1041.

169 D. Suckau, A. Resemann, M. Schuerenberg, P. Hufnagel, J. Franzen and A. Holle, *Anal. Bioanal. Chem.*, 2003, **376**, 952–965.

170 T. A. Zimmerman, D. Debois, G. Mazzucchelli, V. Bertrand, M. C. De Pauw-Gillet and E. De Pauw, *Anal. Chem.*, 2011, **83**, 6090–6097.

171 D. Calligaris, R. Longuespée, D. Debois, D. Asakawa, A. Turtoi, V. Castronovo, A. Noël, V. Bertrand, M. C. De Pauw-Gillet and E. De Pauw, *Anal. Chem.*, 2013, **85**, 2117–2126.

172 S. Tamara, A. Dyachenko, K. L. Fort, A. A. Makarov, R. A. Scheltema and A. J. R. Heck, *J. Am. Chem. Soc.*, 2016, **138**, 10860–10868.

173 T. P. Cleland, C. J. DeHart, R. T. Fellers, A. J. VanNispen, J. B. Greer, R. D. LeDuc, W. R. Parker, P. M. Thomas, N. L. Kelleher and J. S. Brodbelt, *J. Proteome Res.*, 2017, **16**, 2072–2079.

174 S. M. Greer and J. S. Brodbelt, *J. Proteome Res.*, 2018, **17**, 1138–1145.

175 X. Dang and N. L. Young, *Proteomics*, 2014, **14**, 1128–1129.

176 P. Mallick, M. Schirle, S. S. Chen, M. R. Flory, H. Lee, D. Martin, J. Ranish, B. Raught, R. Schmitt, T. Werner, B. Kuster and R. Aebersold, *Nat. Biotechnol.*, 2007, **25**, 125–31.

177 M. R. Groseclose, M. Andersson, W. M. Hardesty and R. M. Caprioli, *J. Mass Spectrom.*, 2007, **42**, 254–262.

178 M. Ronci, S. Sharma, T. Chataway, K. P. Burdon, S. Martin, J. E. Craig and N. H. Voelcker, *J. Proteome Res.*, 2011, **10**, 3522–3529.

179 H. C. Diehl, B. Beine, J. Elm, D. Trede, M. Ahrens, M. Eisenacher, K. Marcus, H. E. Meyer and C. Henkel, *Anal. Bioanal. Chem.*, 2015, **407**, 2223–2243.

180 D. E. Clemmer and M. F. Jarrold, *J. Mass Spectrom.*, 1997, 32, 577–592.

181 M. C. Djidja, E. Claude, M. F. Snel, P. Scriven, S. Francese, V. Carolan and M. R. Clench, *J. Proteome Res.*, 2009, **8**, 4876–4884.

182 J. Stauber, L. MacAleese, J. Franck, E. Claude, M. Snel, B. K. Kaletas, I. M. V. D. Wiel, M. Wisztorski, I. Fournier and R. M. a Heeren, *J. Am. Soc. Mass Spectrom.*, 2010, **21**, 338–47.

183 Y. Schober, T. Schramm, B. Spengler and A. Römpp, *Rapid Commun. Mass Spectrom.*, 2011, **25**, 2475–2483.

184 B. Heijs, R. J. Carreira, E. A. Tolner, A. H. De Ru, A. M. J. M. Van Den Maagdenberg, P. A. Van Veelen and L. A. McDonnell, *Anal. Chem.*, 2015, **87**, 1867–1875.

185 J. Franck, M. El Ayed, M. Wisztorski, M. Salzet and I. Fournier, *Anal. Chem.*, 2009, **81**, 8305–8317.

186 P. J. Brownridge, V. M. Harman, D. M. Simpson and R. J. Beynon, in *Methods in molecular biology (Clifton, N.J.)*, 2012, vol. 893, pp. 267–293.

187 T. Porta, A. Lesur, E. Varesio and G. Hopfgartner, *Anal. Bioanal. Chem.*, 2015, **407**, 2177–2187.

188 M. Komatsu, Y. Murayama and H. Hashimoto, *Appl. Surf. Sci.*, 2008, **255**, 1162–1164.

189 J. Seuma, J. Bunch, A. Cox, C. McLeod, J. Bell and C. Murray, *Proteomics*, 2008, **8**, 3775–84.

190 J. S. Becker, A. Matusch, C. Palm, D. Salber, K. A. Morton and J. S. Becker, *Metallomics*, 2010, **2**, 104–111.

191 C. Giesen, T. Mairinger, L. Khoury, L. Waentig, N. Jakubowski and U. Panne, *Anal. Chem.*, 2011, **83**, 8177–8183.

192 C. Giesen, H. A. O. Wang, D. Schapiro, N. Zivanovic, A. Jacobs, B. Hattendorf, P. J. Schüffler, D. Grolimund, J. M. Buhmann, S. Brandt, Z. Varga, P. J. Wild, D. Günther and B. Bodenmiller, *Nat. Methods*, 2014, **11**, 417–422.

193 J. S. Becker, A. Matusch and B. Wu, *Anal. Chim. Acta*, 2014, **835**, 1–18.

194 J. Olejnik, E. Krzymañska-Olejnik and K. J. Rothschild, *Methods Enzymol.*, 1998, **291**, 135–154.

195 G. Thiery, R. L. Mernaugh, H. Yan, J. M. Spraggins, J. Yang, F. F. Parl and R. M. Caprioli, *J. Am. Soc. Mass Spectrom.*, 2012, **23**, 1689–1696.

196 J. Franck, K. Arafah, M. Elayed, D. Bonnel, D. Vergara, A. Jacquet, D. Vinatier, M. Wisztorski, R. Day, I. Fournier and M. Salzet, *Mol. Cell. Proteomics*, 2009, **8**, 2023–2033.

197 and I. F. J. Stauber, R. Lemaire, M. Wisztorski, S.Ait-Menguellet, J. P. Lucot, D. Vinatier, A. Desmond, M. Deschamps, G. Proess, I. Rudlof, M. Salzet, in *HUPO 5th Annual World Congress*, p. 2006.

198 G. Thiery, M. S. Shchepinov, E. M. Southern, A. Audebourg, V. Audard, B. Terris and I. G. Gut, *Rapid Commun. Mass Spectrom.*, 2007, **21**, 823–829.

199 H. M. Santos and J. L. Capelo, *J. Proteomics*, 2012, **75**, 4921–4930.

200 M. S. Shchepinov and V. a Korshun, *Chem. Soc. Rev.*, 2003, **32**, 170–180.

201 G. Thiery, E. Anselmi, A. Audebourg, E. Darii, M. Abarbri, B. Terris, J. C. Tabet and I. G. Gut, *Proteomics*, 2008, **8**, 3725–3734.

202 J. Yang, P. Chaurand, J. L. Norris, N. a Porter and R. M. Caprioli, *Anal. Chem.*, 2012, **84**, 3689–95.

203 R. Hong, J. True and C. Bieniarz, *Anal. Chem.*, 2014, **86**, 1459–1467.

204 M. van de Waterbeemd, K. L. Fort, D. Boll, M. Reinhardt-Szyba, A. Routh, A. Makarov and A. J. R. Heck, *Nat. Methods*, 2017, **14**, 283–286.

205 H. Li, H. H. Nguyen, R. R. Ogorzalek Loo, I. D. G. Campuzano and J. A. Loo, *Nat. Chem.*, 2018, **10**, 139–148.

206 L. S. Eberlin, X. Liu, C. R. Ferreira, S. Santagata, N. Y. R. Agar and R. G. Cooks, *Anal. Chem.*, 2011, **83**, 8366–8371.

207 H. Thiele, S. Heldmann, D. Trede, J. Strehlow, S. Wirtz, W. Dreher, J. Berger, J. Oetjen, J. H. Kobarg, B. Fischer and P. Maass, *Biochim. Biophys. Acta - Proteins Proteomics*, 2014, **1844**, 117–137.

208 B. Heijs, W. M. Abdelmoula, S. Lou, I. H. Briaire-de Bruijn, J. Dijkstra, J. V. M. G. Bovée and L. A. McDonnell, *Anal. Chem.*, 2015, **87**, 11978–11983.

209 W. M. Abdelmoula, R. J. Carreira, R. Shyti, B. Balluff, R. J. M. van Zeijl, E. A. Tolner, B. F. P. Lelieveldt, A. M. J. M. van den Maagdenberg, L. A. McDonnell and J. Dijkstra, *Anal. Chem.*, 2014, **86**, 3947–3954.